UC-20F

RENSSELAER POLYTECHNIC INSTITUTE

PLASMA DYNAMICS LABORATORY

TROY, NEW YORK 12181

"RECENT BEAM PROBE MEASUREMENTS ON EBT, TMX, AND RENTOR"

BY

R. L. HICKOK

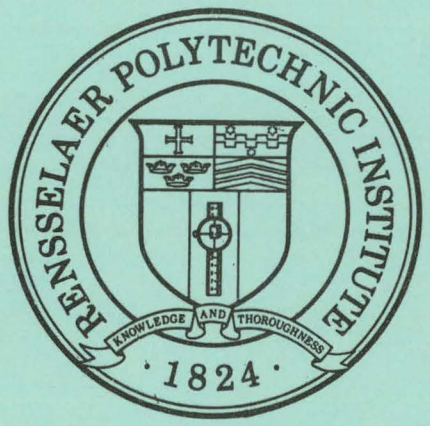

REPORT NO: DOE/ET.53004-4

RPDL REPORT NO. 80-13

JUNE 1980

DISCLAIMER

DISCLAIMER

Printed in the United States of America
Available from
National Technical Information Service
U.S. Department of Commerce
5285 Port Royal Road
Springfield, VA 22161

NTIS price code
Printed Copy: $6.00
Microfiche copy: A01

PAGES i to ii

WERE INTENTIONALLY

LEFT BLANK

CONTENTS

		PAGE
I.	INTRODUCTION	1
II.	BASIC DESCRIPTION OF BEAM PROBING	1
III.	EBT BEAM PROBE MEASUREMENTS	13
IV.	TMX RESULTS	25
V.	RENTOR MEASUREMENTS	34
VI.	SUMMARY	42
	DISTRIBUTION LIST	45

RECENT BEAM PROBE MEASUREMENTS ON EBT, TMX, AND RENTOR

R. L. Hickok

I. INTRODUCTION

This report is based on an invited paper presented at the High Temperature Plasma Diagnostic Conference held in Los Angeles in March 1980. The format follows the talk in that the text is primarily a discussion of the Figures. A brief review of beam probes is presented in Section II and Sections III, IV, and V present results from EBT, TMX, and RENTOR.

II. BASIC DESCRIPTION OF BEAM PROBING

Fig. 1 gives a list of people who have made contributions to the development of heavy ion beam probing. Fig. 2 is a short table that indicates why we are interested in beam probing. Our group at RPI has used beam probes to measure n, T_e, ϕ and fluctuations in n and ϕ. McCormick and Kick at Garching have measured J(r) with a Li beam probe. Simulation studies clearly indicate that beam probing can provide useful information about β. It may also be possible to obtain information about T_i by making use of charge exchange reactions or by observing line radiation emitted by the probing beam.

Fig. 3 shows a simplified sketch of the type of beam probing I am going to be talking about. A beam of singly charged ions are directed across the magnetic field and through the plasma. Some of these primary ions undergo impact ionization collisions with the plasma electrons to form doubly charged secondary ions. There is a fan of secondary ions emerging from the plasma

COLLABORATORS:

F. C. JOBES
J. F. MARSHALL
R. A. DANDL
R. S. HORNADY

R.P.I. STAFF:

W. C. JENNINGS
K. A. CONNOR
J. T. WOO
J. F. LEWIS

POST DOCS:

J. STUFFLEBEAM
P. COLESTOCK
S. KUO
C. PARSONS
J. PIPKINS
R. KLINKOWSTEIN
A. HERSHCOVITCH
F. BIENIOSEK

GRADUATE STUDENTS:

J. HUCHITAL
R. REINOVSKY
J. GLOWIENKA
G. HALLOCK
C. FIORE
J. KOLAWOLE
K. POURREZAEI
W. KOSTENKO
M. REED
T. PRICE
R. SCARPETTI
F. BRESNOCK
J. ANTONIADES
G. TONETTI
L. SOLENSTEN
P. SCHOCH
K. SAADATMAND

ADM. STAFF:

R. RAFUN
A. HAYNER

FIGURE 1

WHY BEAM PROBING

PARAMETER	IS BEAM PROBE SENSITIVE?
N	YES
I_E	YES
T_I	?
Φ	YES
β	YES
J(R)	YES
FLUCTUATIONS	YES

FIGURE 2

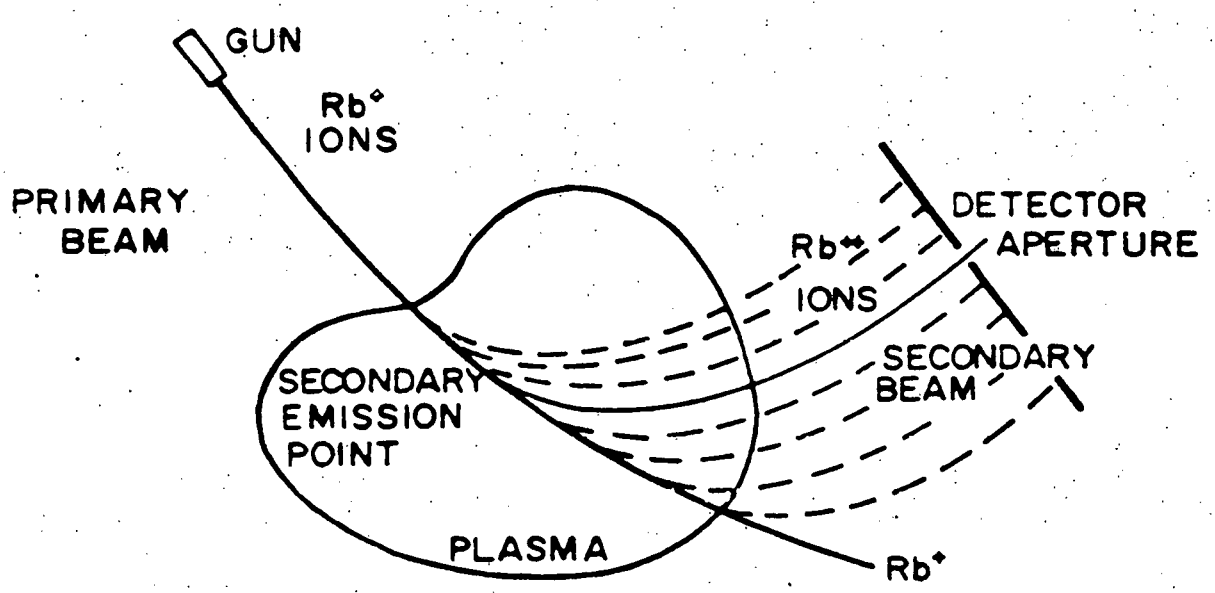
GUN
Rb+
IONS
PRIMARY
BEAM
DETECTOR
APERTURE
Rb+
IONS
SECONDARY
BEAM
SECONDARY
EMISSION
POINT
PLASMA
Rb+

FIGURE 3

that are separated from the primary beam by the magnetic field. By using a small aperature detector, we look only at those secondary ions created in a small sample volume located at some preselected point on the primary beam path.

Fig. 4 shows two types of measurements that can be made with this diagnostic. The intensity of the secondary ion beam current is given by

$$I_s = \Gamma n_e f(T_e)$$

where Γ is a known or calculable geometric factor, n_e is the plasma electron density at the sample point, and $f(T_e)$ is the effective cross section for the reaction. If the electron temperature is known, then n_e can be evaluated or conversely if n_e is known then T_e can be evaluated. There are two techniques that can be used to separately evaluate n and T_e. The same point in the plasma can be probed with two different primary ion species that have different $f(T_e)$ values. Generally this is only useful for low temperature plasmas (< 50 eV). A second technique makes use of the fact that in addition to creating 2^+ secondary ions, collisions with the plasma electrons can also generate 3^+, 4^+, and higher charge states (3^+ and 4^+ states have been observed). These multiple ionization reactions have different temperature dependence and, consequently can be used to separate n and T_e. I don't really know what upper temperature range can be investigated by this technique since most of the multiple ionization cross sections are unknown.

The bottom part of Fig. 4 illustrates the technique for measuring the space potential. The primary beam enters the plasma and climbs up the space potential hill. In doing so it loses an energy $e\phi$. On exiting the plasma,

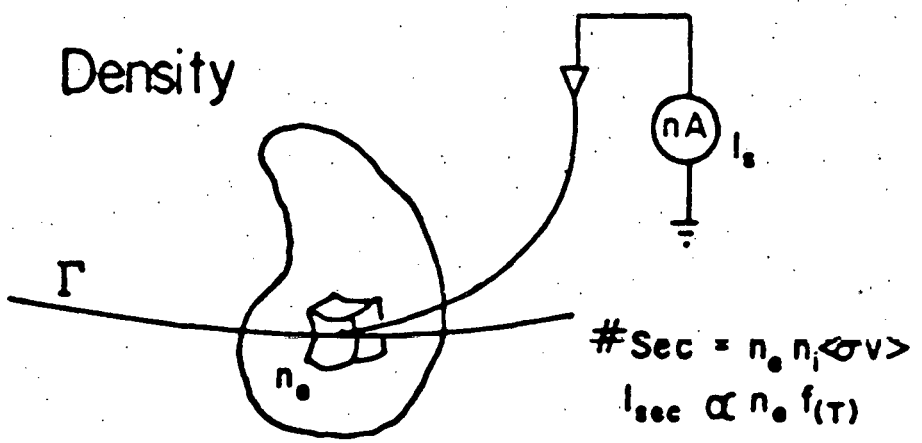
Density
nA
I_s
Γ
n_e
#Sec = $n_e n_i \langle \sigma v \rangle$
$I_{sec} \propto n_e f_{(T)}$

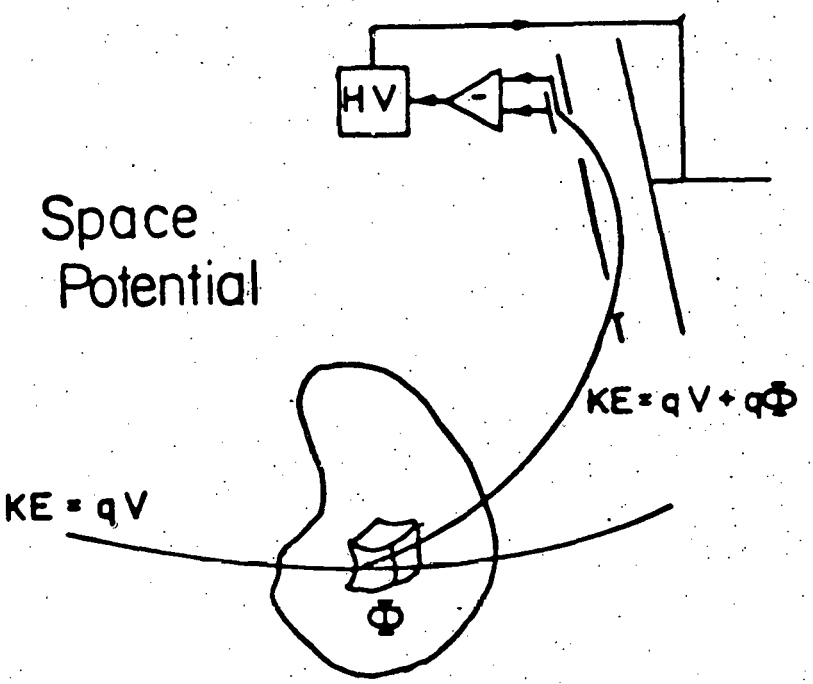
HV
Space
Potential
KE = qV + qΦ
KE = qV
Φ

FIGURE 4

the doubly charged secondary ions gain an energy of $2e\phi$; so the difference in energy between the primary and secondary ions is just $e\phi$. By using a feedback controlled parallel plate electrostatic energy analyzer, this energy difference can be measured to about 1 part in 10^4.

Figure 5 shows a very simplified diagram of the essential parts of a beam probe system. Starting in the upper left hand corner is a slaving system that gets inputs about the magnetic field, the mass of the ion being used and the desired sweep voltage. The slaving system sends out signals to a sweep amplifier and to a programmable high voltage supply that drives an ion gun. The selected beam energy and sweep voltage determines a unique trajectory for the primary beam and the detector location selects a unique sample volume on this primary beam trajectory. The intensity of both the primary and secondary beams are transmitted to some recording system along with information on the beam energy and sweep voltage.

If the sweep voltage is now varied, then the observation point will be swept through the plasma along a path called the detector line. This is indicated by the line marked E3, E4 in the diagram. If the beam energy is changed, then it will move the detector line. Increasing the beam energy moves the detector line towards the gun, and decreasing it moves it away from the gun. Thus the beam energy and the sweep voltage determines a unique observation point in the plasma.

Typical operating parameters for present day beam probe systems are beam energies in the 10 - 100 kV range, and beam currents in the 10 - 100 μA range. This produces secondary ion currents in the one to a few hundred nanoampere range depending upon the plasma density and temperature. Typical

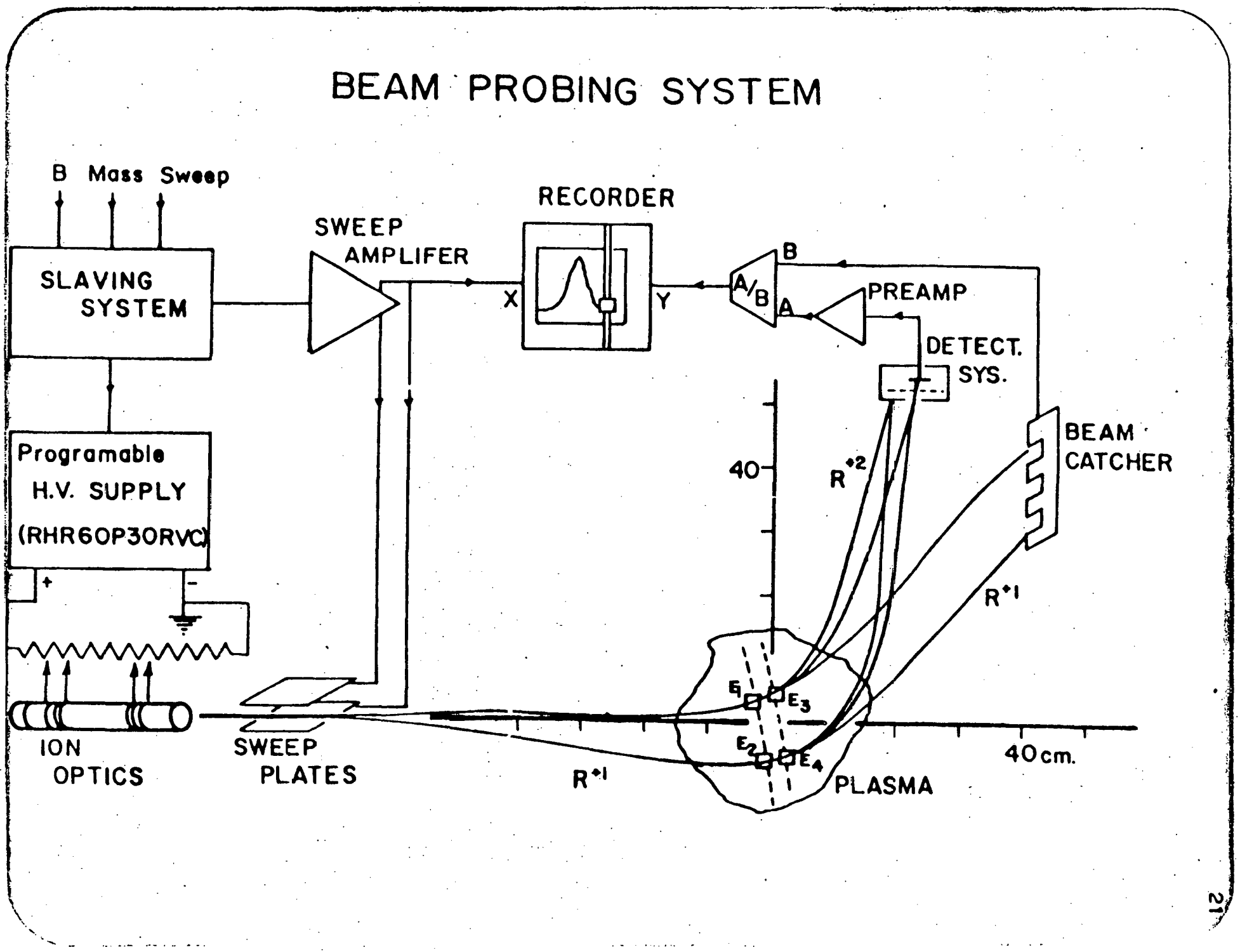
BEAM PROBING SYSTEM
B Mass Sweep
SLAVING SYSTEM
SWEEP AMPLIFER
RECORDER
X
Y
A/B
B
A
PREAMP
DETECT. SYS.
BEAM CATCHER
Programable H.V. SUPPLY (RHR60P30RVC)
+
-
40
R+2
R+1
E1
E3
E2
E4
ION OPTICS
SWEEP PLATES
R+1
PLASMA
40cm.

FIGURE 5

space resolution is of the order of one-half a cubic centimeter and time resolution of $nf(T_e)$ measurements is of the order of 1 microsecond. Time resolution of space potential measurements is generally somewhat slower due to the slow frequency response of the high gain feedback loop of the electrostatic energy analyzer. Frequency response for space potential measurements is generally in the range of 10 - 50 kilohertz. Density and space potential profiles along the detector line can be made in less than one millisecond. Moving the detector line by changing the beam energy is a somewhat slower process due to the slow slew rate of the high voltage power supplies. It is possible to completely automate the mapping of the plasma cross section by programming both the sweep amplifier and the high voltage power supplies.

Figure 6 shows the effective cross section for the ionization of a 20 kilovolt rubidium plus beam from the 1^+ to the 2^+ state as a function of electron temperature. Note that in the 5 - 50 eV range, this is a very sensitive function of electron temperature, but above 100 eV the cross section is relatively constant. At high electron temperatures above a few hundred eV, the cross section slowly decreases. The cross section is also inversely proportional to the beam velocity, so that the effective cross section has to be evaluated for the specific beam velocity that is being used.

Figure 7 shows an isometric sketch of a parallel plate electrostatic energy analyzer that is the heart of the space potential measurements. This is basically a standard electrostatic energy analyzer, except that we use a wide exit aperature and split plate detectors. The signals from the two

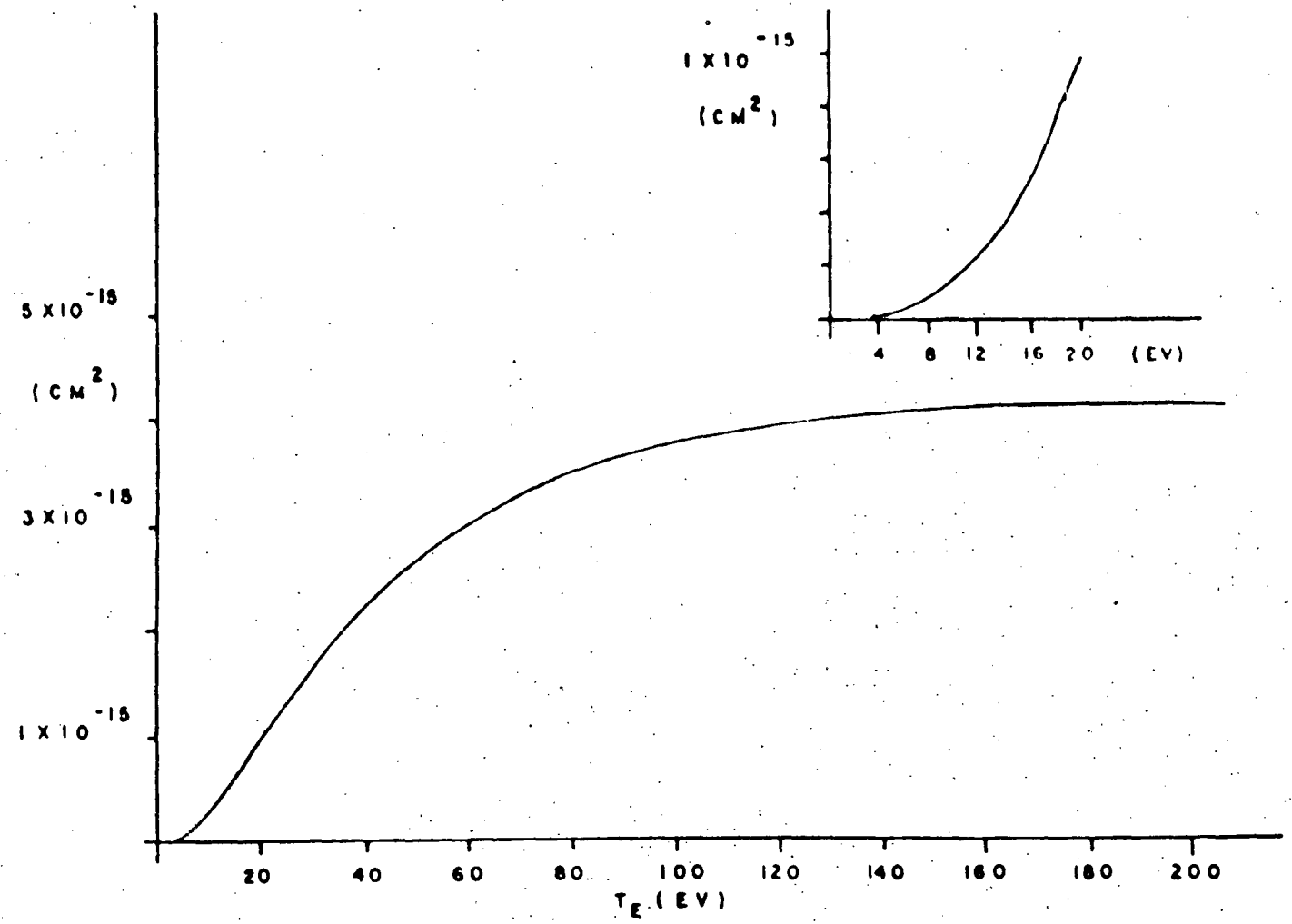
1 X 10 -15
(CM 2)
4 8 12 16 20 (EV)
5 X 10 -15
(CM 2)
3 X 10 -15
1 X 10 -15
20 40 60 80 100 120 140 160 180 200
T E (EV)

FIGURE 6

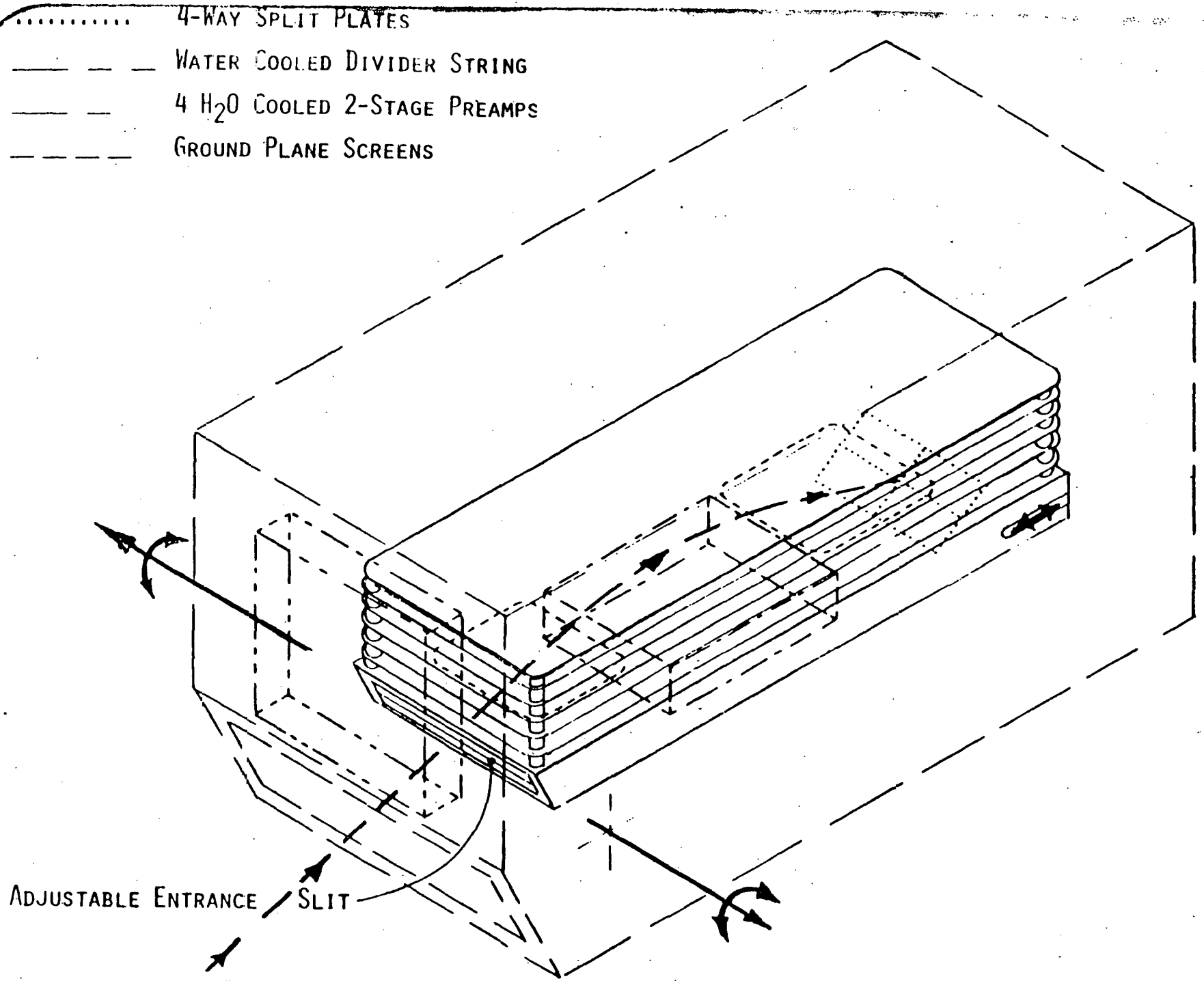
4-WAY SPLIT PLATES
WATER COOLED DIVIDER STRING
4 H_2O COOLED 2-STAGE PREAMPS
GROUND PLANE SCREENS
ADJUSTABLE ENTRANCE SLIT

FIGURE 7

split plates are passed through a difference amplifier, a high gain, high voltage amplifier, and then fed back to the top plate of the analyzer. This balances the current on the two split plates and when the system is set up properly, the feedback voltage is directly proportional to the space potential at the point under observation. Generally the detector plates are split four ways, i.e., left-right as well as up-down, as this provides a convenient way for centering the beam in the left-right direction in the analyzer. If the magnetic field was purely in the z direction, then the beam trajectories would be a two dimensional problem; but generally there are some non-z components to the field and this produces some z deflection of the beam. For example, on Tokamaks there is the poloidal field; on TMX there are some quadrapole components to the field; and on EBT there are radial field components. They produce a z deflection of the beam which is detected by observing the difference in current between the left-right plates. This difference signal can then be coupled back to z steering plates on the primary beam and used to center the beam in the analyzer.

The analyzer is also sensitive to the angle at which the beam enters the analyzer. As the observation point is scanned through the plasma, the secondary ion beam will enter the analyzer at different angles and this has to be corrected for. The analyzers that we presently use have a nominal design entrance angle of 30° which provides second order focusing. In setting the system up, we provide for rotation of the complete analyzer about the entrance slit in order to position it at the design angle. The preamplifiers and the high voltage divider string for the analyzer guard rings are mounted inside the analyzer's shield box. This minimizes the length of the

low level signal leads and high voltage feed through. The signals are at relatively high level when they are brought out through the vacuum wall. All electrical and mechanical connections are brought out through the rotating pivot arms so that the complete analyzer and shield box rotates as a single unit. The mechanical connections permit adjustment of the entrance slit from outside the vacuum chamber and for adjusting the distance between the entrance slit and the split plate detectors.

Figure 8 shows a typical set of angular correction curves for one of these analyzers. These particular curves were taken during the testing of the TMX analyzer. The curves are uniquely determined by the ratio of the horizontal separation between the detector plates and the entrance slit to the vertical distance of the detector plates below the ground plane. The three curves shown were obtained by varying the horizontal separation between the entrance slit and the detector plates. In general we would not like to correct the data for the angular variation in the entrance angle. Consequently, the system is set up to provide minimum correction over the required acceptance angle for the specific experiment. This introduces a small systematic error in the space potential profiles which can be corrected for, if necessary.

III. EBT BEAM PROBE MEASUREMENTS

Figure 9 shows a schematic diagram of the beam probe system installed on EBT. At the top is an ion gun which can operate up to 60 kilovolts. The gun chamber is isolated from the main system by a vacuum valve so that we can change ion sources without bringing the whole system up to atmosphere.

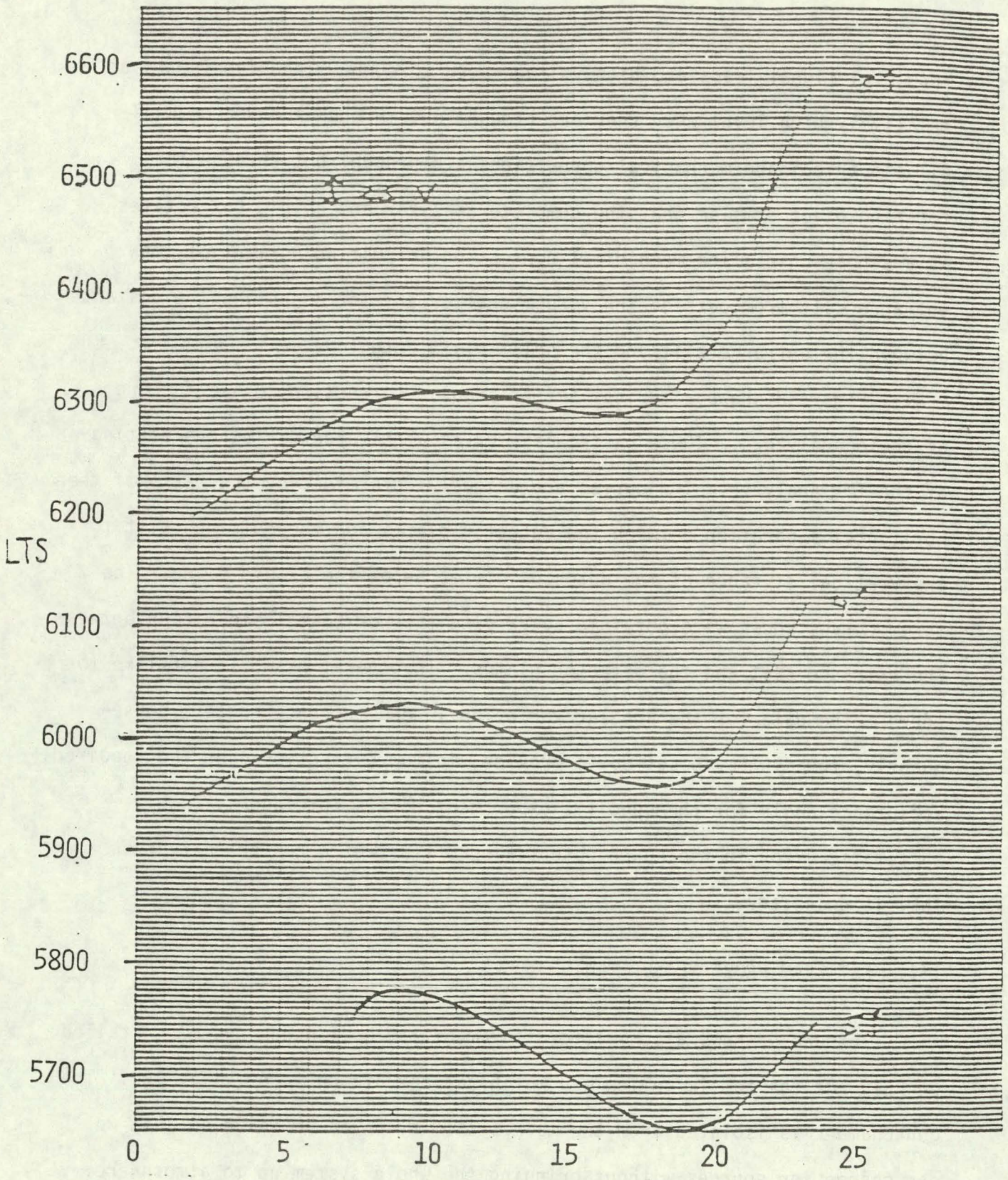
6600
6500
6400
6300
6200
LTS
6100
6000
5900
5800
5700
0
5
10
15
20
25
ANGULAR POSITION (DEGREES)

FIGURE 8

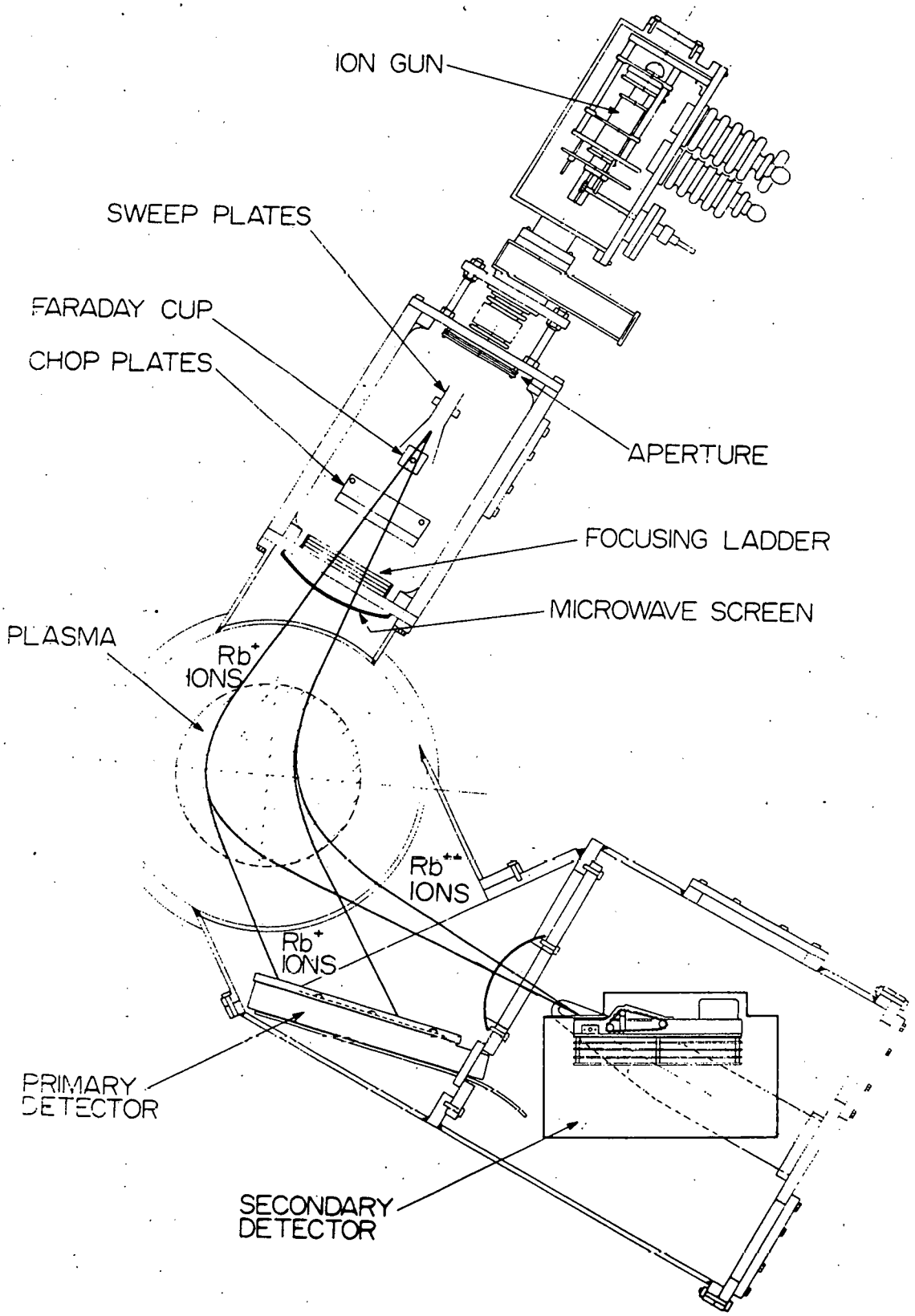
ION GUN
SWEEP PLATES
FARADAY CUP
CHOP PLATES
APERTURE
FOCUSING LADDER
MICROWAVE SCREEN
PLASMA
Rb+ IONS
Rb++ IONS
Rb+ IONS
PRIMARY DETECTOR
SECONDARY DETECTOR

FIGURE 9.

There is a limiting aperature to define the beam as it enters the optics chamber. Next comes a set of sweep plates for sweeping the beam across the plasma. There is a Faraday cup which can be moved in and out of postion in order to monitor the primary beam current. In this particular system there is also a set of chopped plates so that we can chop the beam and use phase sensitive detection in order to improve the signal-to-noise ratio. This is followed by a focusing ladder which is a series of wires used to monitor the beam focusing characteristics. The beam then passes through a microwave screen which is used to keep the high microwave power of EBT from getting into the optics and gun chamber. The beam then passes through the plasma where the secondary ions are created and they follow trajectories which bring them into the electrostatic energy analyzer. The detector chamber is also isolated from the main EBT vacuum system by a microwave screen. A primary detector is also indicated, but this is only used in the absence of the plasma. The primary detector is too noisy when there is plasma in the system. Two typical primary beam paths and two typical secondary ion trajectories are shown in the diagram.

For calibration purposes, the system is set up to bend the primary path into the analyzer. The analyzer voltage is then adjusted to center the primary beam on the split plate detectors and is then slaved to the ion gun. When making measurements with the secondary ions, a precise gain of one-half amplifier is introduced into the feedback loop to compensate for the 2^{+} charge on the secondary ions.

Figure 10 shows a grid map for the EBT beam probe system. The lines running up and down labeled from -500 to +500 correspond to observation

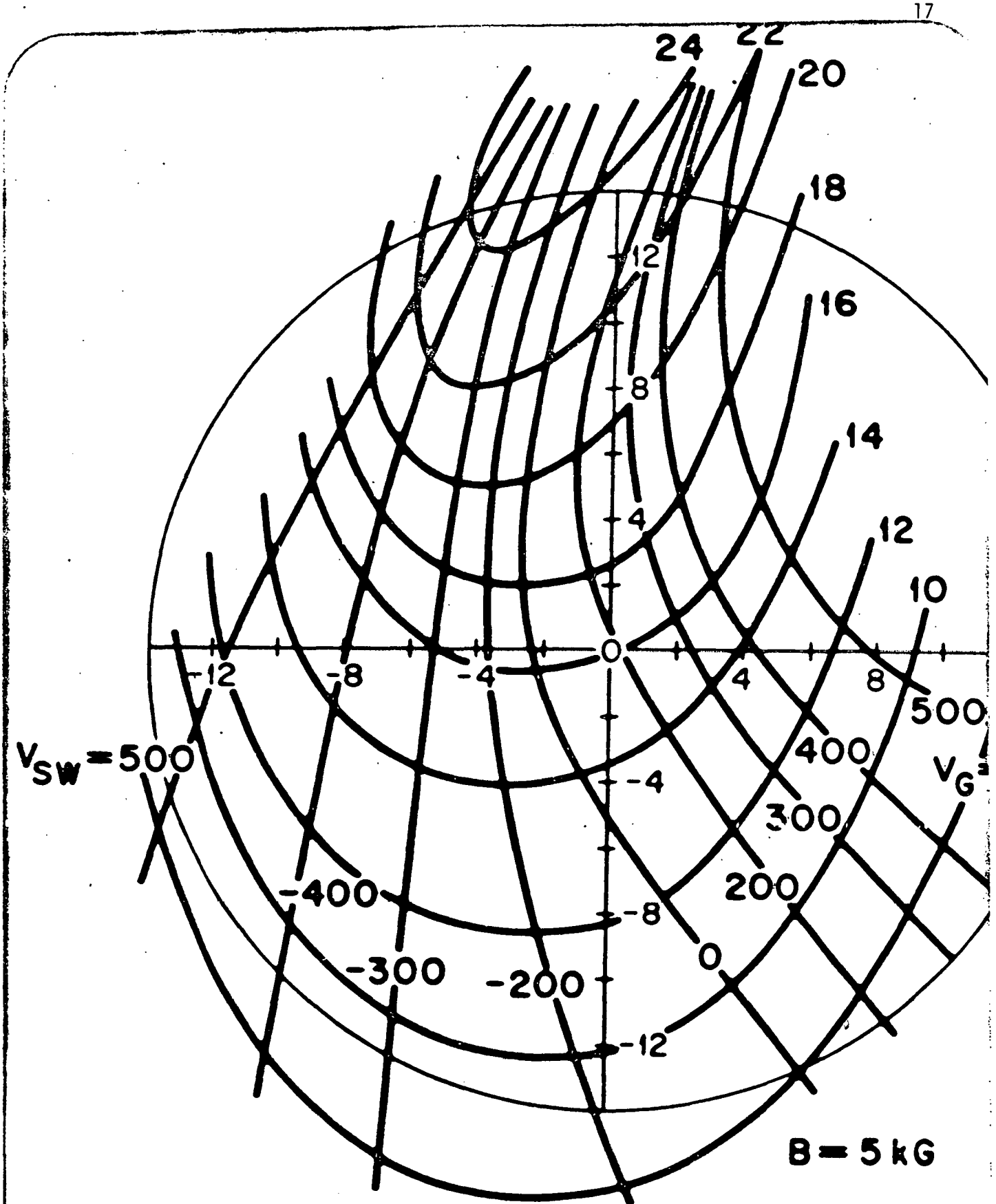

GRID MAP

FIGURE 10

points at fixed sweep voltage, but varying beam energy. The lines running from left to right labeled from 8 to 24 are the detector lines for a fixed beam energy, but varying sweep voltage. Thus by picking the appropriate beam energy and sweep voltage, we can look at any specific spot in the plasma. Ideally we would prefer a nice rectangular grid since the sample volume depends on the angle between the primary beam paths and the detector lines. In general this is not possible, and the sample volume changes as we move the observation point through the plasma. This difference in sample volume has to be corrected for when analyzing the nf(T) data, but it does not effect the space potential measurements.

Figure 11 shows an early space potential profile obtained on EBT. This is a beam energy scan and corresponds to walking along a nearly vertical line labeled zero in Fig. 10. This is a rather crude measurement by our present standards, but it was the first indication of the negative potential well in EBT.

Figure 12 is also some early EBT data. This is an isometric drawing of the negative potential well observed in EBT. In constructing this isometric map, a lot of smoothing was done on the data. It illustrates the more or less symmetric potential well that is obtained when EBT is run in the T mode of operation. Figure 13 is some recent data showing much more detail about the potential structure. This contour map illustrates the detail that is now possible with this beam probe system. The contour lines correspond to 25 volt steps in the space potential. At the center the potential is about 75 volts negative with respect to the wall, and increases in a reasonably symmetric manner out to zero potential. The

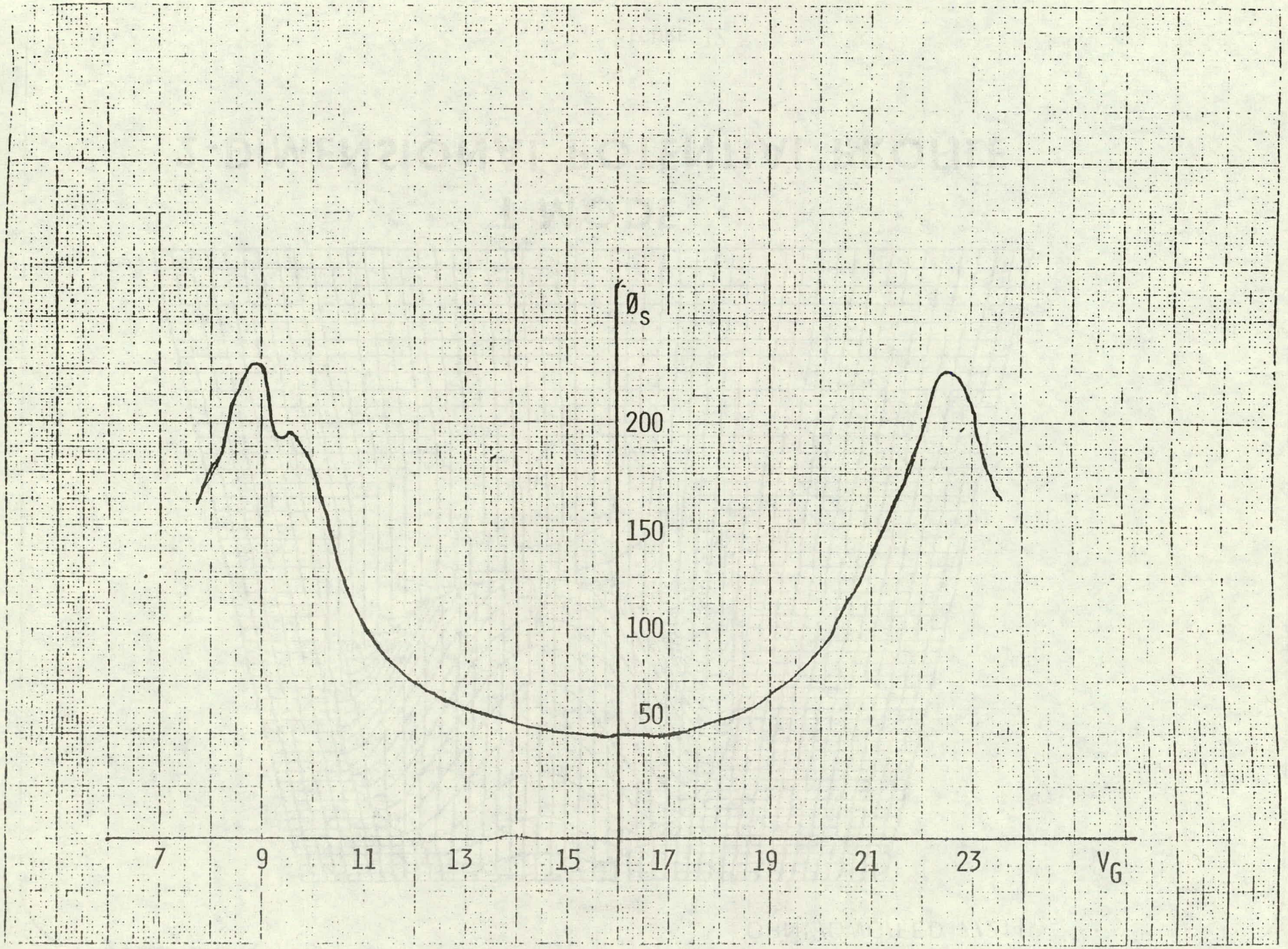

FIGURE 11

ORNL/DWG/FED-77214

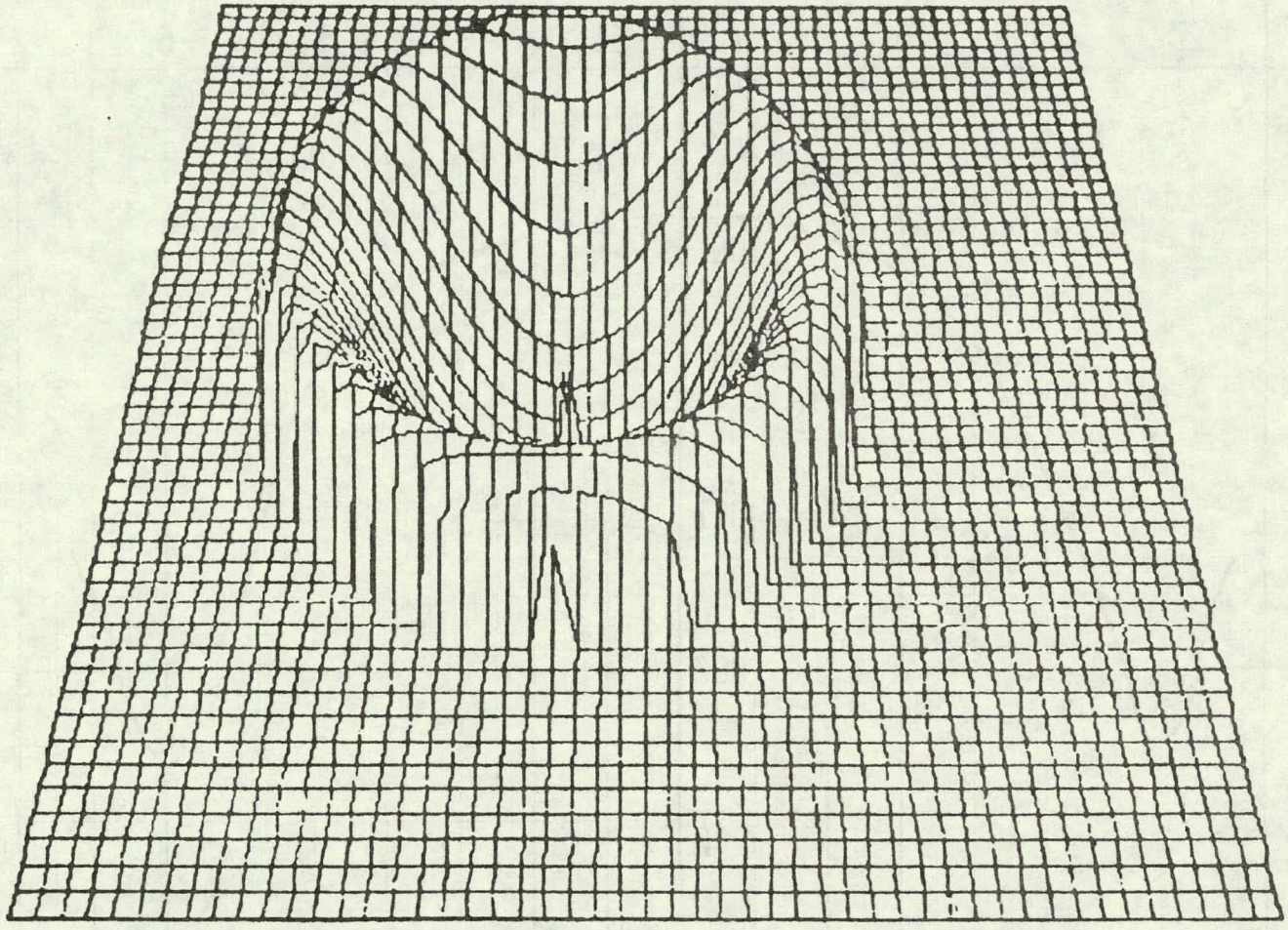

T MODE

2-DIMENSIONAL POTENTIAL PROFILE

FIGURE 12

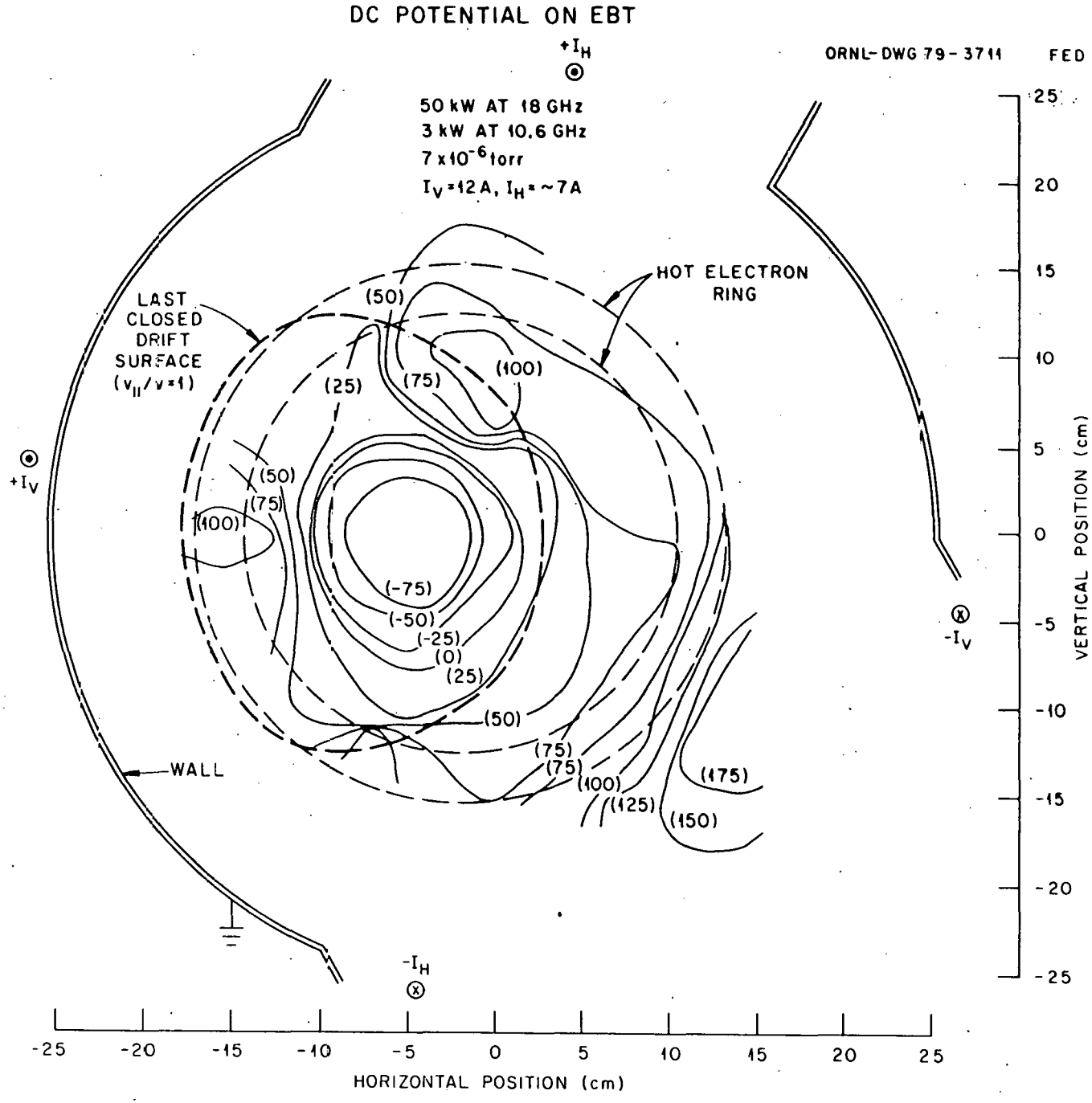
DC POTENTIAL ON EBT
ORNL-DWG 79-3711 FED
+I_H
50 kW AT 18 GHz
3 kW AT 10.6 GHz
7 x 10^-6 torr
I_V = 12 A, I_H = ~7A
HOT ELECTRON RING
LAST CLOSED DRIFT SURFACE (v_||/v = 1)
+I_V
-I_V
-I_H
WALL
(50)
(25)
(75)
(100)
(-75)
(-50)
(-25)
(0)
(125)
(150)
(175)
VERTICAL POSITION (cm)
HORIZONTAL POSITION (cm)
25
20
15
10
5
0
-5
-10
-15
-20
-25

FIGURE 13

potential continues to increase as you move out radially, but the symmetry becomes distorted. Note that at the top and bottom and left and right, we have indicated the position of the horizontal and vertical correction coils that are used to suppress the toroidal current in EBT. With a little imagination, you may be able to correlate the breakdown in the symmetry with the location of the horizontal and vertical correction coils. We hope to investigate this in more detail to find out if the correction coils are indeed influencing the space potential profiles.

As I mentioned earlier, it is also possible to generate 3^+, 4^+, and higher ionization states. Figure 14 illustrates this on the EBT. This shows results obtained with a rubidium beam at a fixed energy and scanning the top plate voltage of the electrostatic energy analyzer. The 3^+ and 4^+ signals are easily observed as well as the normal 2^+ signals. Note that there is a difference in gain of a factor of 30 between the 2^+ and the 3^+ and 4^+ signals. It should also be noted that the various multiple ionization states are coming from different regions in the plasma. In principle it should be possible to use the $3^+ - 2^+$ ratio to evaluate the electron temperature, but this is a very difficult analysis. This ratio however, can be used to provide some information about the ring region in EBT, and this is illustrated in Fig. 15. The top curve shows a typical space potential profile from near the center of the vacuum chamber out to a radius of approximately 24 centimeters. The lower curve shows the change in the 3^+ to 2^+ ratio as we scan across the ring region. The shaded vertical line shows the region of the second harmonic for the 18 GHz rf power. The maximum in the so-called halo curve, appears to lie just outside the second harmonic zone. But Bieniosek

Relative Intensity of 2^+, 3^+, and 4^+ Signals

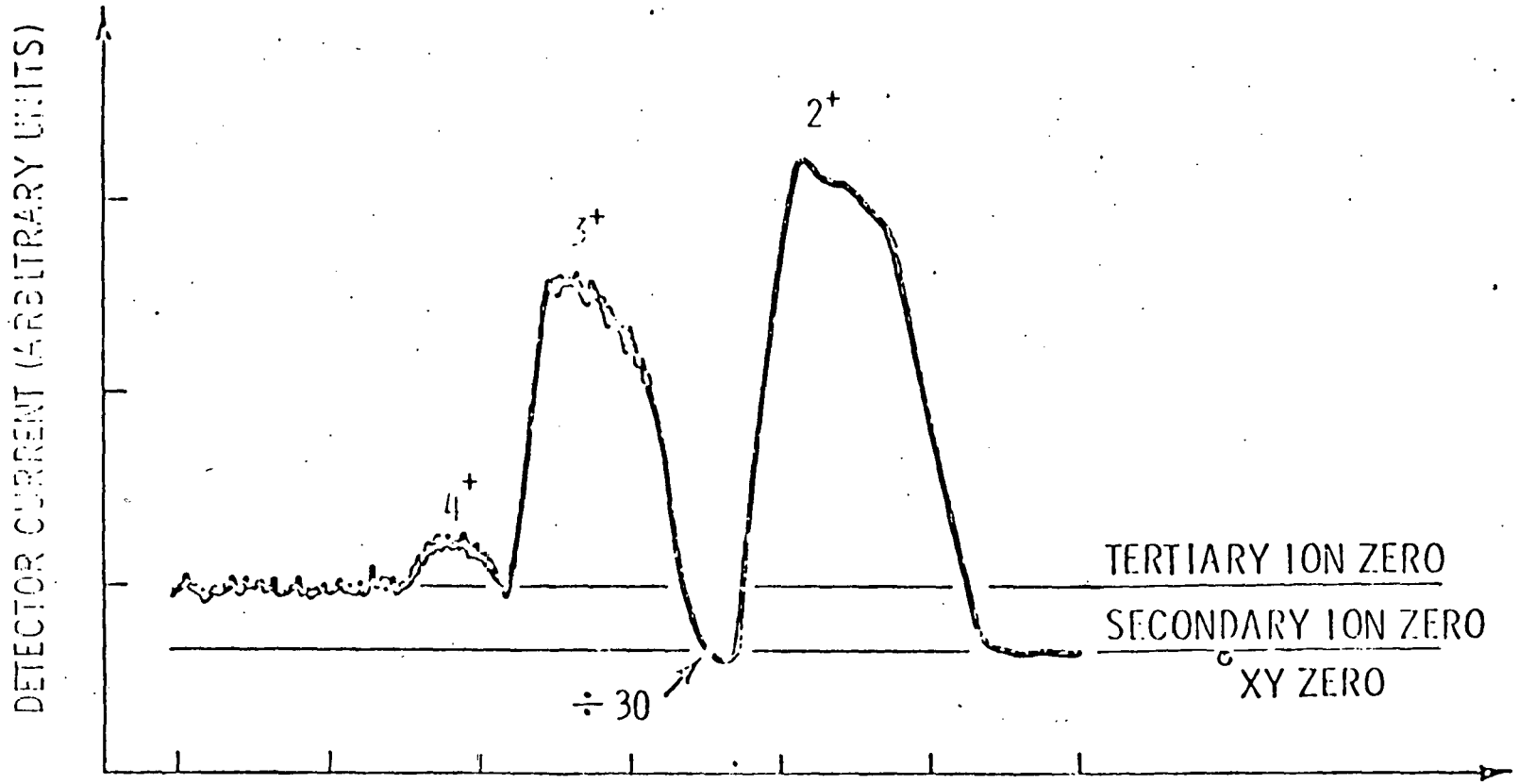

ANALYZER SCAN

Figure 14

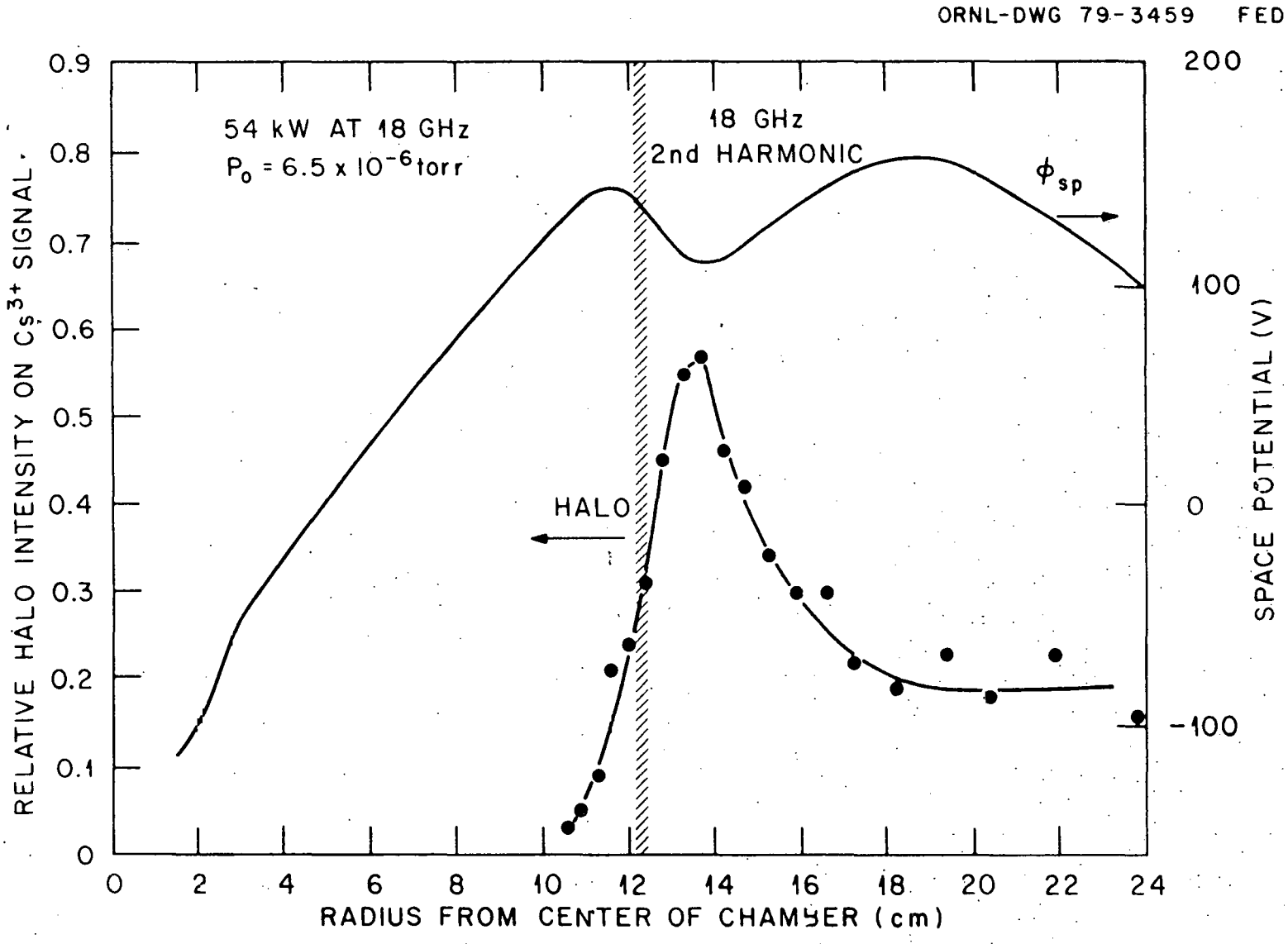
ORNL-DWG 79-3459 FED
54 kW AT 18 GHz
$P_o = 6.5 \times 10^{-6}$ torr
18 GHz
2nd HARMONIC
ϕ_{sp}
HALO
RELATIVE HALO INTENSITY ON Cs^{3+} SIGNAL
SPACE POTENTIAL (V)
RADIUS FROM CENTER OF CHAMBER (cm)
0
0.1
0.2
0.3
0.4
0.5
0.6
0.7
0.8
0.9
200
100
0
-100
0
2
4
6
8
10
12
14
16
18
20
22
24

FIGURE 15

in a more detailed analysis of this curve (in a paper being presented at this conference), shows that this ratio must be corrected for the change in temperature of the cold background plasma as a function of radius. This correction shifts the halo curve towards the center and it actually lines up with the second harmonic heating zone.

IV. TMX RESULTS

Figure 16 shows a detailed schematic of the beam probe system installed on the center cell of TMX. This is the most sophisticated beam probe system in operation today. The system is fully computer controlled and the signals from the four way split plates in the analyzer are automatically digitized and stored in the computer for off-line analysis. The analyzer can also be operated in the conventional analog feedback control mode to provide on-line display of the density and space potential signals. Not all of the automation has been fully implemented yet, but the system is operational. The first signals from the system were only obtained last August, so the quantity and quality of data is not anywhere near as extensive as it is on EBT. Figure 17 shows the energy angle detection grid for the vacuum field of TMX. The solid lines represent constant energy, angular sweep detection lines. The dashed lines represent constant sweep voltage variable beam energy lines. One of the problems that had to be considered with the TMX beam probe was that this plasma system was designed to operate at relatively high β and high potential. Both of these factors can distort the energy angle detection grid. This is illustrated in Fig. 18. In calculating this detection grid, we assumed a β of one-half with a square well

HEAVY ION BEAM PROBE

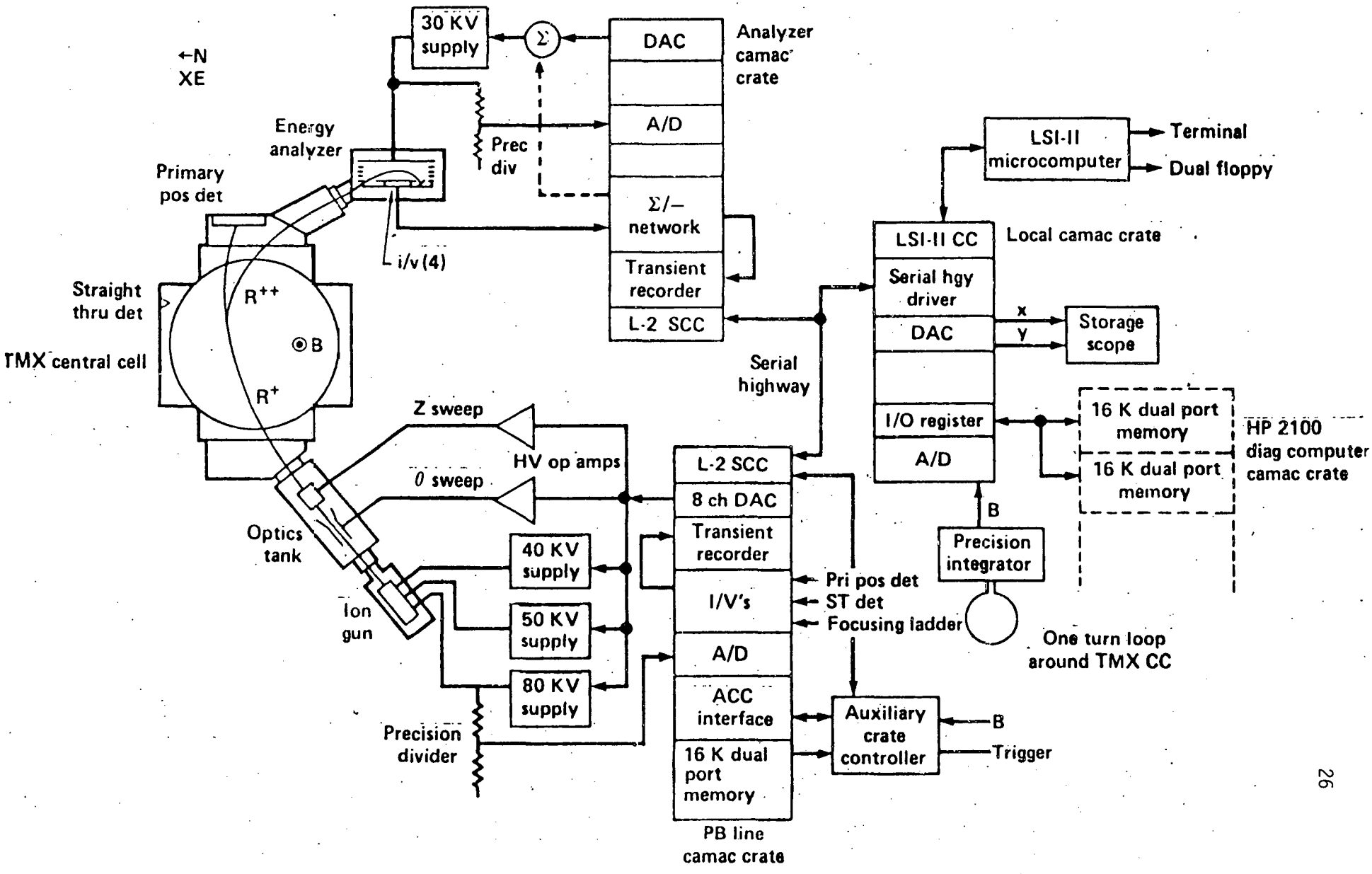

FIGURE 16

ENERGY-ANGLE DETECTION GRID BETA = 0 POTENTIAL = 0

Ion: K
Energy: 12.4 – 18.4 kV
Azimuth: 121 – 137 deg
Polar: 90 deg

XO: 70.0 cm
YO: –140.0 cm
XDET: 125.0 cm
YDET: 171.0 cm

Plasma radius: 30 cm
B: 500.0 gauss

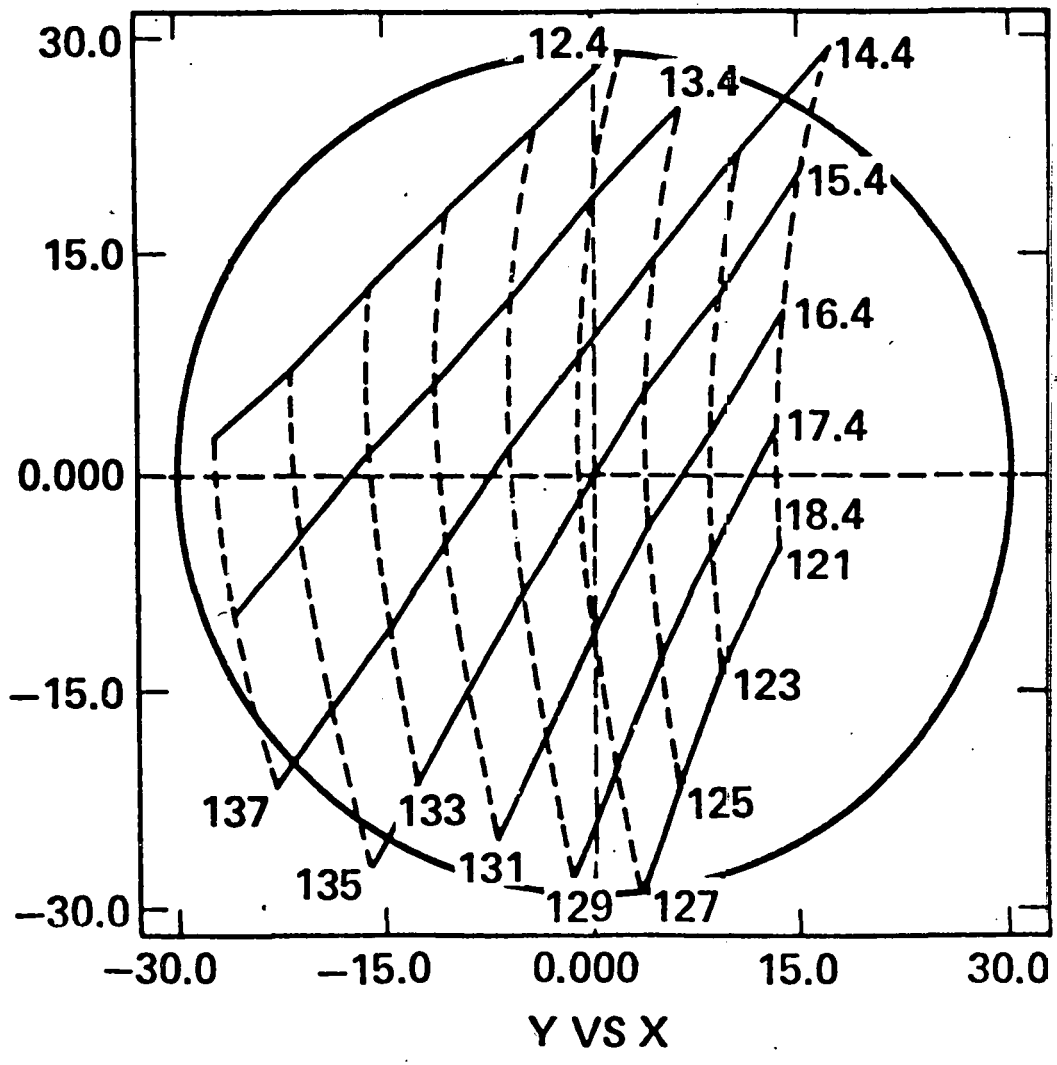

FIGURE 17

ENERGY-ANGLE DETECTION GRID
BETA = 0.5 POTENTIAL = 1000 V

Ion: K
Energy: 12.1 – 13.2 kV
Azimuth: 122 – 134 deg
Polar: 90 deg

XO: 70.0 cm
YO: –140.0 cm
XDET: 125.0 cm
YDET: 171.0 cm

Plasma radius: 30.0 cm
B: 500.0 gauss

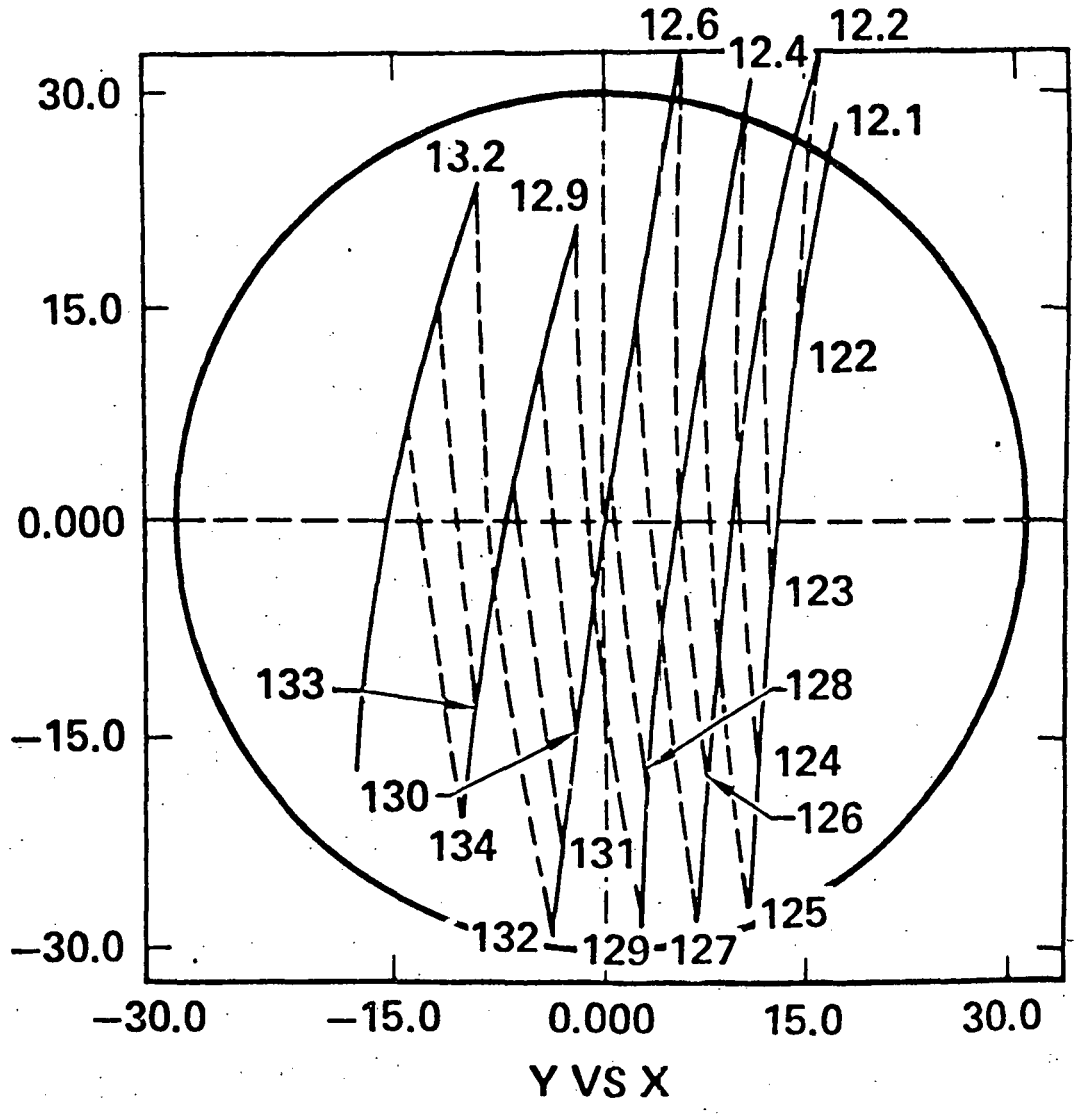

FIGURE 18

profile out to a radius of 30 centimeters and flux conservation inside the vacuum chamber. The potential was assumed flat at 1000 volts out to a radius of 20 centimeters with a Gaussian fall off with a 5 centimeter half-width. You can see that this condition seriously distorts the detection grid. All of the measurements can still be made, but we lose track of the location of the sample volume in the plasma that is providing the secondary ion signal. What has to be done is to make a number of scans across the plasma and then use an iteration technique on the trajectory calculations in order to obtain a self-consistent picture. Fortunately, or perhaps unfortunately, TMX has not been run under these extreme conditions. Most of the measurements have been made at higher vacuum magnetic field where the β is only a few percent and the potential is of the order of a few hundred volts. For these conditions, there is very little distortion from the vacuum field grid.

Figure 19 shows some unprocessed secondary signals from TMX. The beam is being swept in the z direction across the analyzer, and the spikes that you see on the four split plate signal photographs are the secondary ion signals. You will note that the signals are riding on top of a small, nearly dc offset. This offset is produced by a 50 ampere neutral hydrogen diagnostic beam in the center cell. This beam should not enter the analyzer, and if it did enter the analyzer it would have the wrong energy to strike the detection plates. But we are looking at nanoampere levels and there is enough scattered signal from the 50 ampere beam to provide this small dc offset signal. This was a new source of noise for beam probe systems. In the past, most of our noise problems have been with ultraviolet light coming

UNPROCESSED SECONDARY SIGNALS

Setup

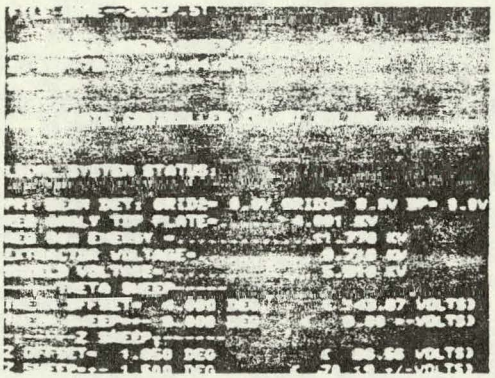

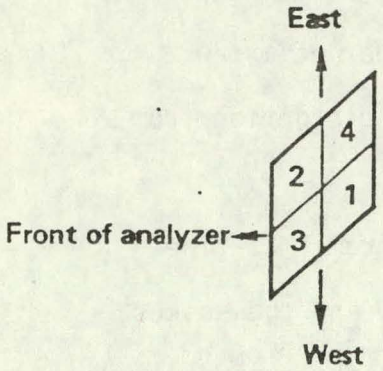

To separate the secondary signal from the background noise the beam is chopped east-west across the split plates. This is done by sweeping the primary beam with the "z" plates. Note that in this shot the beam is swept too far west – out of the analyzer entrance slit. This gives the double peaked signals on plates 1 and 3.

Split plate signals

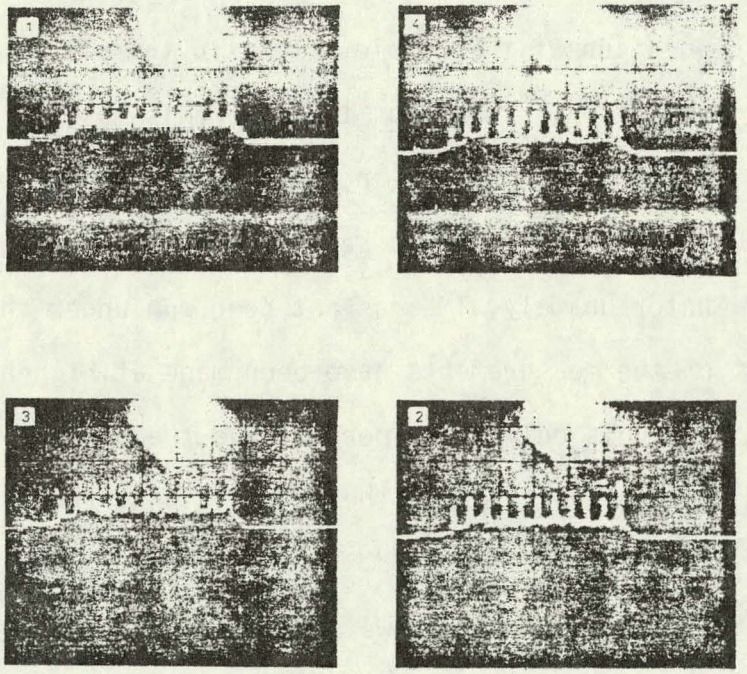

Horizontal: 4 ms/div
Vertical: 20 na/div

FIGURE 19

through the entrance aperature of the analyzer, being scattered onto the detection plates and knocking off secondary electrons. Ultraviolet noise is very hashy in character with a broad frequency spectrum. Fortunately, this dc, or at least nearly dc noise produced by the energetic neutral beam is much easier to deal with. For this data the analyzer was not operated in the feedback control mode, but the top plate voltage was adjusted to provide equal magnitude signals on all four plates.

Figure 20 shows some radial profile data that was taken last December. This data was averaged over a number of shots, but the machine was run under constant conditions to provide nearly the same plasma for each shot. The lines represent the potential at a given point in the plasma as a function of time. The top three lines represent the potential at radial locations of 1 cm, 6.5 cm, and 10 cm. Note that the potential at all three locations is approximately the same. The bottom two lines represents two measurements at a location of 20 cm, and you can see that the potential at the 20 cm radius is considerably less than it is at the 10 cm radius. The potential scale on the left should be read as a relative scale, since we do not yet have a good "absolute" calibration. We are fairly confident that the difference in potential between the 10 cm, 20 cm radial positions, is of the order of 150 volts, but we have very little confidence in the "absolute" values of these potentials with respect to ground. This is strictly a calibration problem. We are in the process of carrying out this calibration and expect to obtain "absolute" values better than 50 volts.

Figure 21 shows some 3^+ thalium ion signals obtained on TMX. They were obtained with a 20 kilovolt thalium beam in a magnetic field of

RADIAL POTENTIAL PROFILE

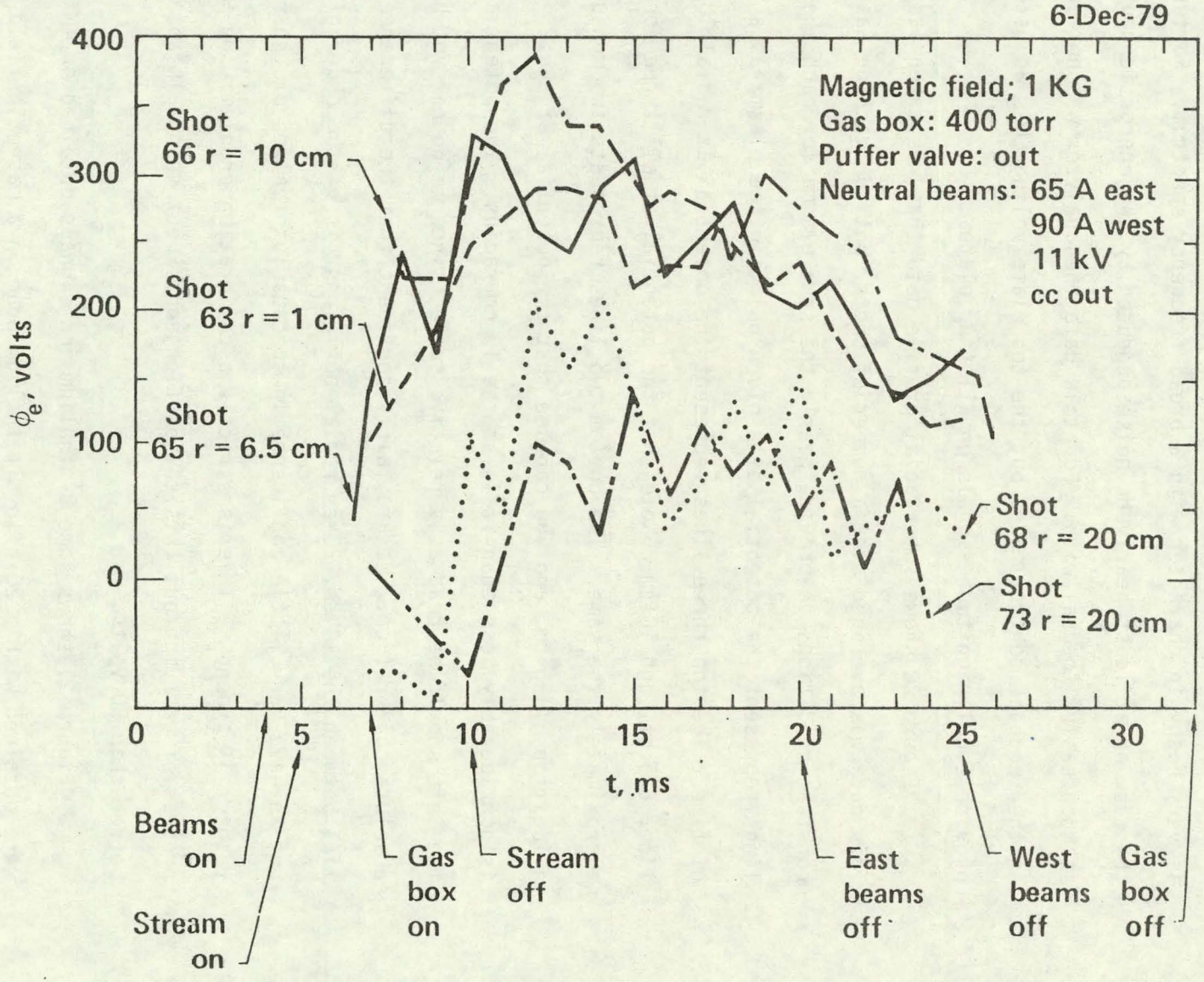

FIGURE 20

TERTIARY SIGNALS

Setup

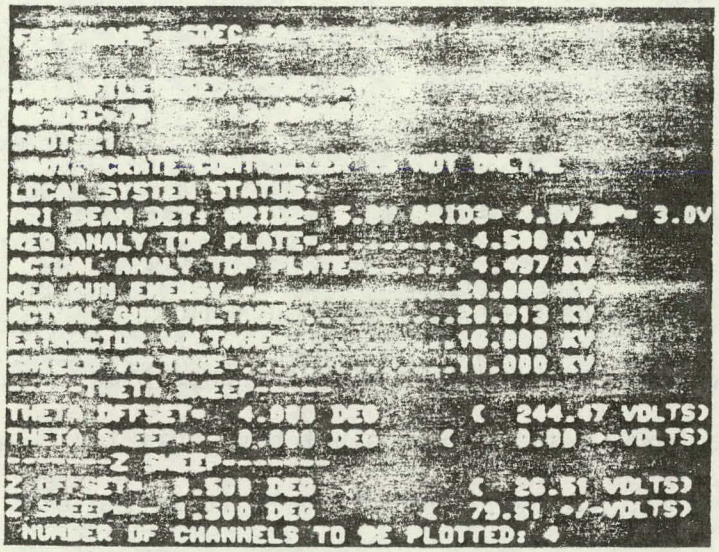

Reaction

$$T\ell^{+} + e^{-} \rightarrow T\ell^{+++} + 3e^{-}$$

Tertiary current level

$$I_t = 3I_p \ell n_e \sigma_{eff,\,t}(T_e)$$

Split plate signals

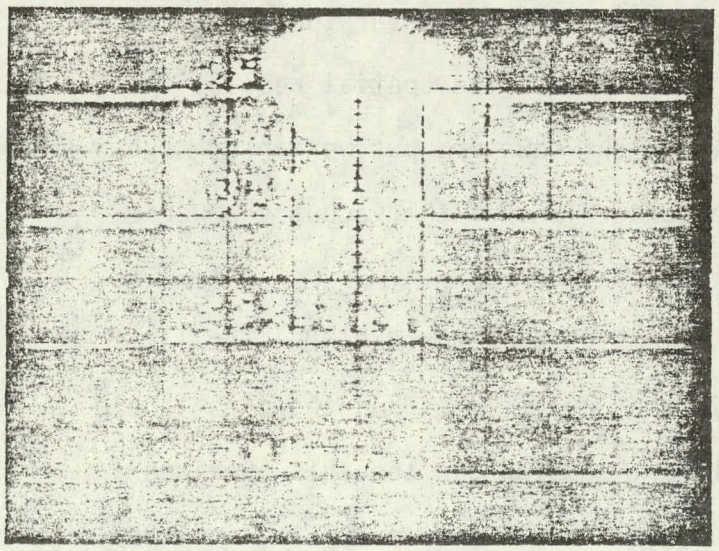

Tertiary data may be combined with secondary data from the same plasma volume to yield a direct measurement of T_e:

SP1

$$\frac{I_s}{I_t} = \frac{2I_p \ell_s n_e \sigma_{eff,\,s}(T_e)}{3I_p \ell_t n_e \sigma_{eff,\,t}(T_e)} = \frac{2\ell_s \sigma_{eff,\,s}(T_e)}{3\ell_t \sigma_{eff,\,t}(T_e)}$$

SP2

SP3

SP4

Horizontal: 4 ms/div Vertical: 100 na/div

FIGURE 21

approximately 1 kilogauss. You can see that for these conditions there is a fairly strong 3^+ signal with very little noise level. Again this is fairly recent data, it is not fully analyzed, we do not have good cross sections for the 1^+ to 3^+ reaction, and we do not have the trajectory calculations to evaluate the size of the sample volume, but it does indicate that the plasma is reasonably hot.

V. RENTOR MEASUREMENTS

Figure 22 shows a schematic of the beam probe system on RENTOR. This is similar to all of the other beam probe systems with the exception of a lens just above the plasma chamber. Actually we do not have this lens installed on RENTOR at the present time, but we plan to install it in the future. This lens structure is generally advantageous on Tokamaks because the 1/R toroidal field has fairly strong focusing properties. The lens moves the effective sweep point close to the plasma and inside the effective focal point of the toroidal field. This prevents strong conversion of the secondary ions as they leave the plasma and improves the spatial resolution. The system can be operated without the lens however, but we cannot make measurements very far inside of the center line of the vacuum chamber. Figure 23 is a photograph of this installation.

Figure 24a shows the energy detection grid for RENTOR. The lines labeled -3° to +7° are constant injection angle lines and the ones labeled 15 to 37 are constant beam energy lines. As you can see this provides an approximately rectangular grid structure, but we cannot map the inner half of the plasma. The bottom curve, Fig. 24b, shows a variation of toroidal

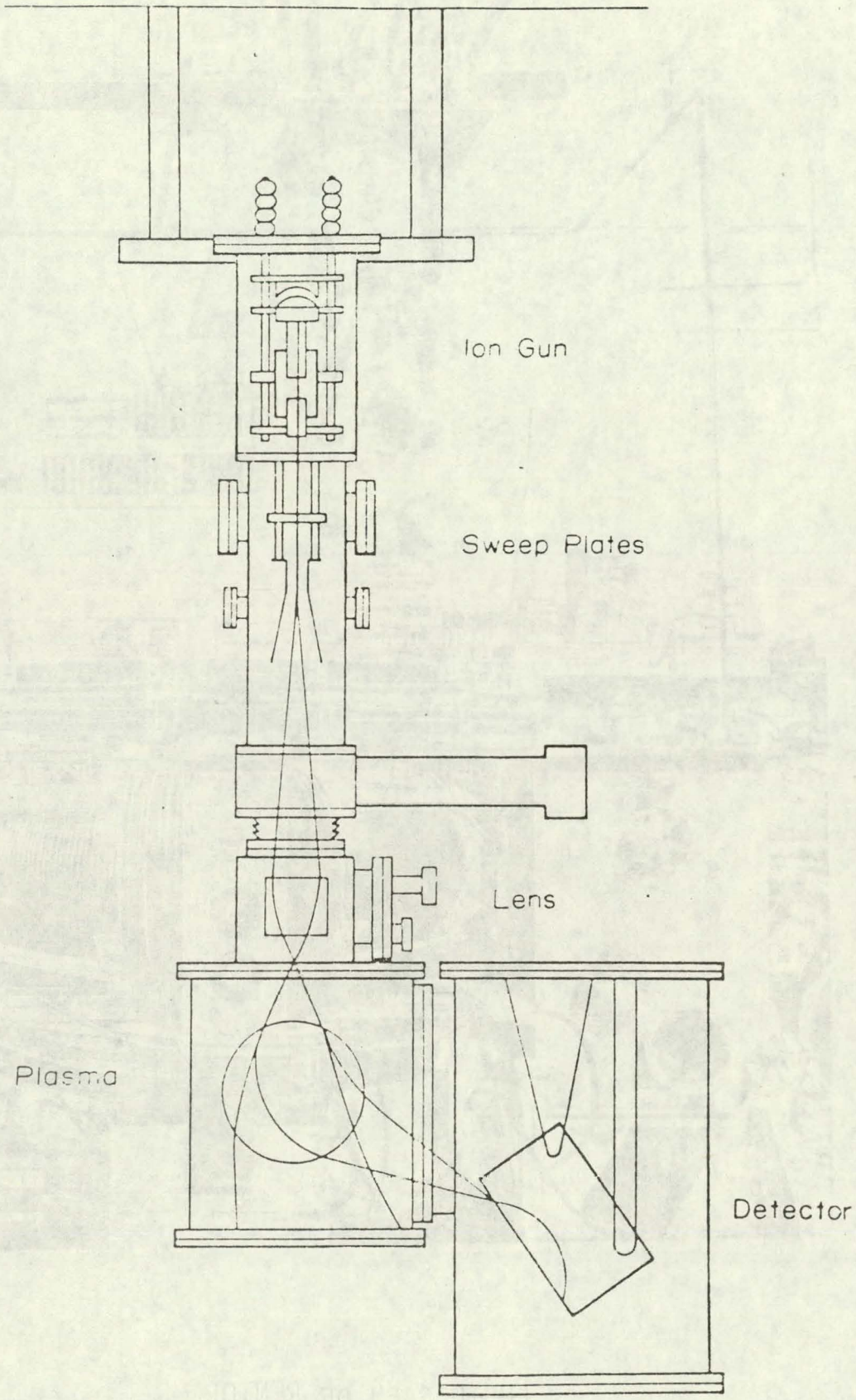

FIGURE 22

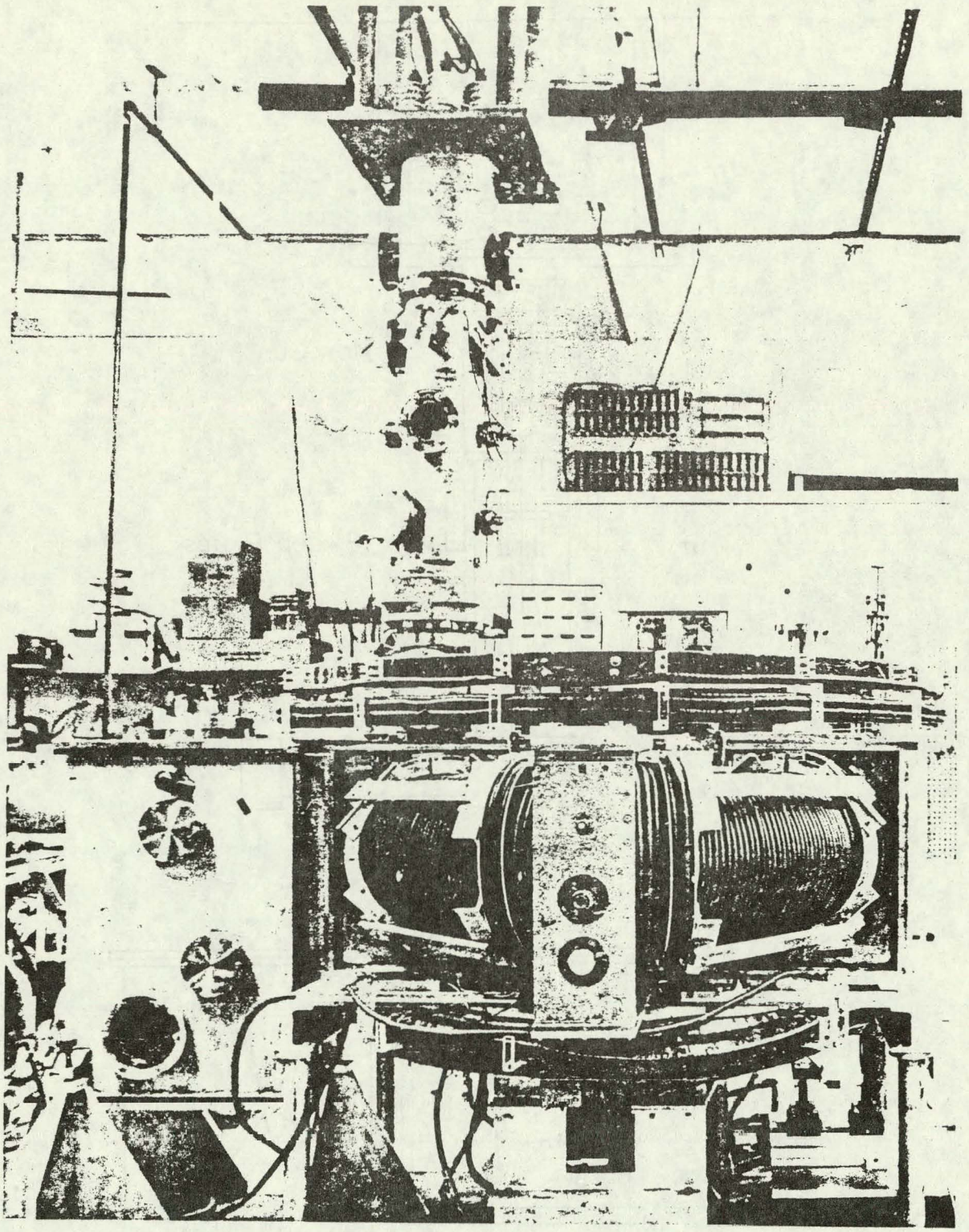

PHOTOGRAPH OF RENTOR

FIGURE 23

FIGURE 24A

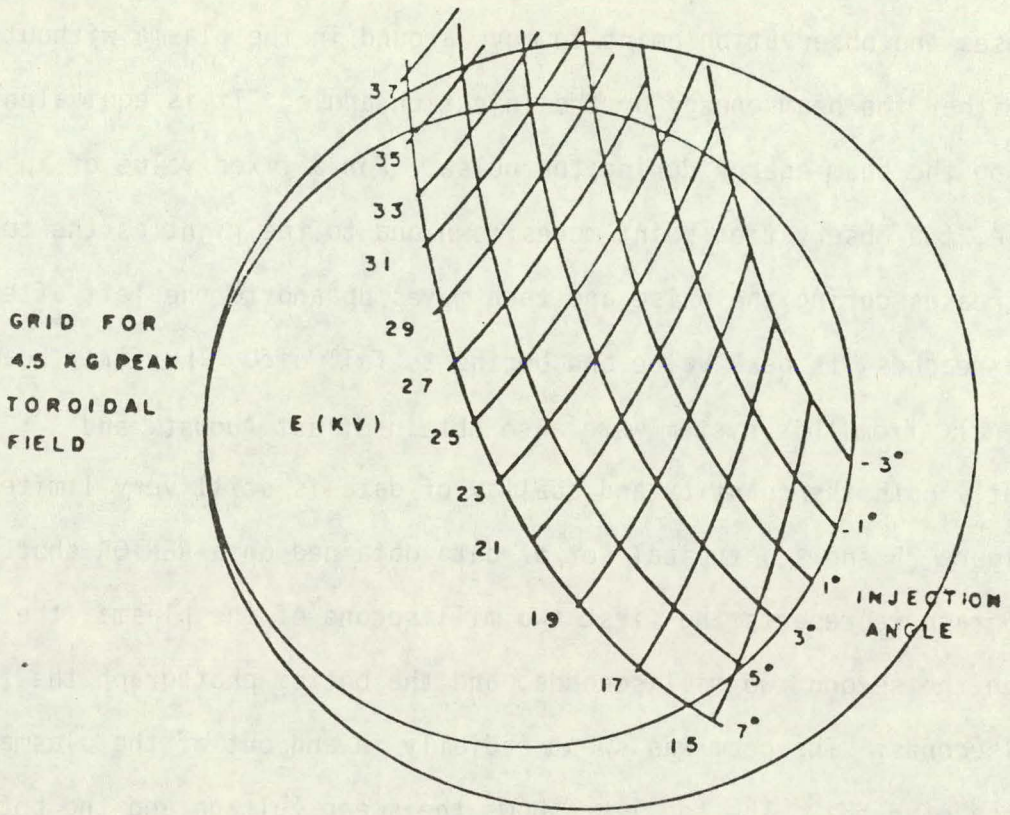

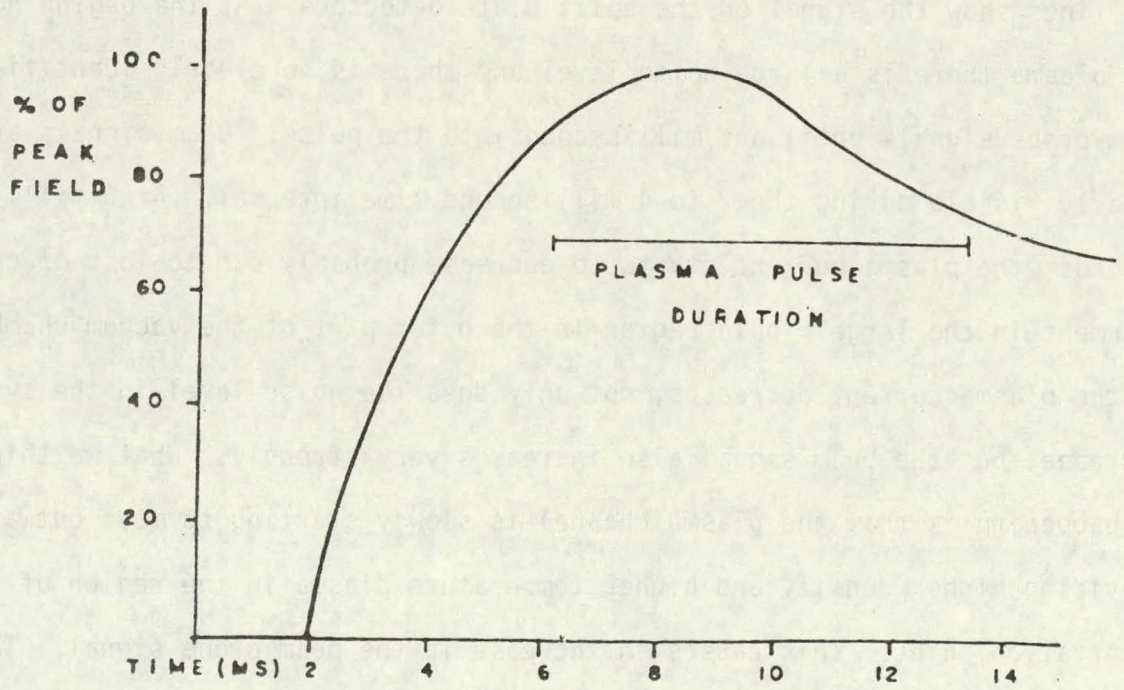

FIGURE 24B

field over the length of the plasma pulse. The strong variation of toroidal field causes the observation point to move around in the plasma without varying either the beam energy or the injection angle. It is equivalent to changing the beam energy during the pulse. For a fixed value of injection angle, the observation point moves down and to the right as the toroidal field increases during the pulse and then moves up and to the left after the field reaches its peak value and begins to fall off. The first beam probe signals from this system were also obtained last August, and consequently both the quantity and quality of data is still very limited.

Figure 25 shows a typical set of data obtained on a RENTOR shot. The top photograph represents the first two millisecond of the plasma, the center photograph the second two milliseconds, and the bottom photograph the final two milliseconds. The beam was swept radially in and out of the plasma at a frequency of 6 KHz. The top line shows the sweep voltage and the bottom two lines show the signal on the split plate detectors. At the beginning of the plasma there is a large noise level and there is no clearly identifiable beam probe signals until one millisecond into the pulse. Beam signals are clearly visible during the 2 to 4 millisecond time interval. At 5 milliseconds, the plasma current starts to decrease probably due to lost of containment in the large ripple region in the outer part of the vacuum chamber. As the plasma current decreases, not only does the noise level in the system increase, but the beam signal also increases very strongly. What we think is happening is that the plasma channel is slowly starting to move outward providing higher density and higher temperature plasma in the region of the observation point. This causes an increase in the beam probe signal. The

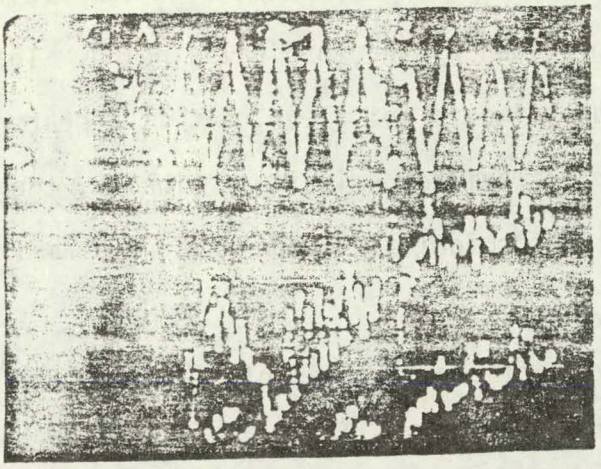

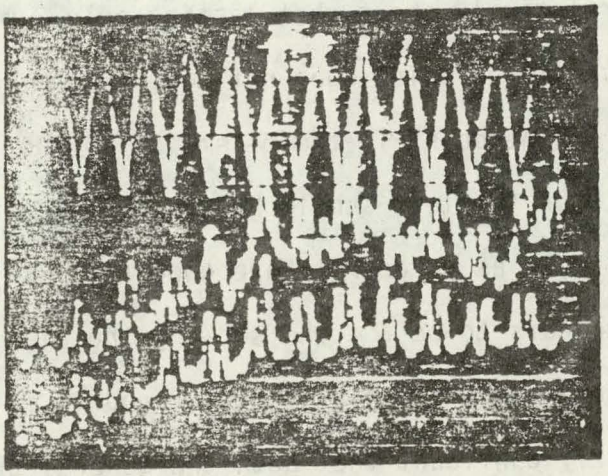

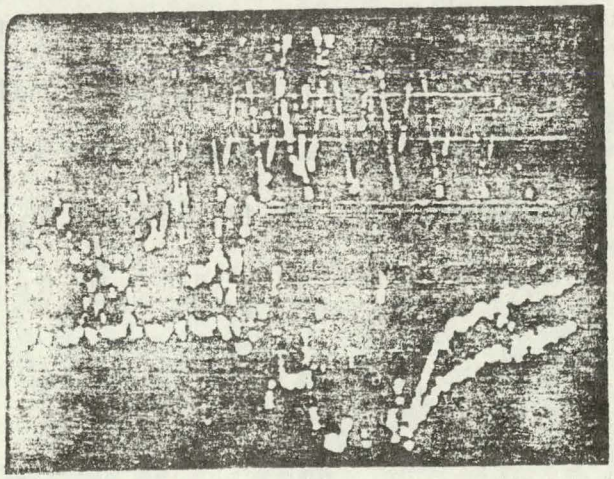

1/5/80 SHOT #108

PANORAMIC VIEW OF THE DETECTOR CHANNELS

RADIAL SWEEP VOLTAGE:
500 V/CM @ 6 KHZ
-482.5 V OFFSET

SECONDARY ION CURRENT:
FRONT SPLIT PLATE:
10 NA/CM
REAR SPLIT PLATE:
10 NA/CM

TIME: 0.2 MS/CM

Rb^+ PRIMARY ION BEAM,
19,420 V

ANALYZER VOLTAGE = 4747 V

FIGURE 25

outward movement is probably due to a decrease in the vertical field since some of the vertical field is provided by the toroidal winding. The reason for the increase in noise at this time is not clear, but it appears that the plasma is generating larger ultraviolet emission. Finally, the plasma current decreases faster than the toroidal field and ends up slamming into the inside wall of the chamber.

Figure 26 shows an analysis of one of the shots taken on RENTOR. We only have an analysis on one of these shots since we are still working on our computer data analysis reduction program and the present analysis is all done by hand. This is a relatively short shot lasting only 3 milliseconds. Consequently, the observation point does not move around very much, and essentially we are looking at one point in the plasma as a function of time. Again the potential scale on the left should be treated as a relative scale and not an"absolute"scale as we do not have good"absolute"calibrations at this time. There appears to be a trend showing the plasma potential decreasing with time. Superimposed on this general trend is fairly large fluctuations. We are fairly confident that both the general trend and the large fluctuations are real. We have not yet attempted to correlate the fluctuations with other diagnostics such as fluctuations on the microwave interferometer, pick up on x-ray detectors, or photodiode signals. At the present time we only claim that the beam probe system does work on the small Rensselaer tokamak. We are confident that it will be able to provide density, temperature, and space potential profile data in the future.

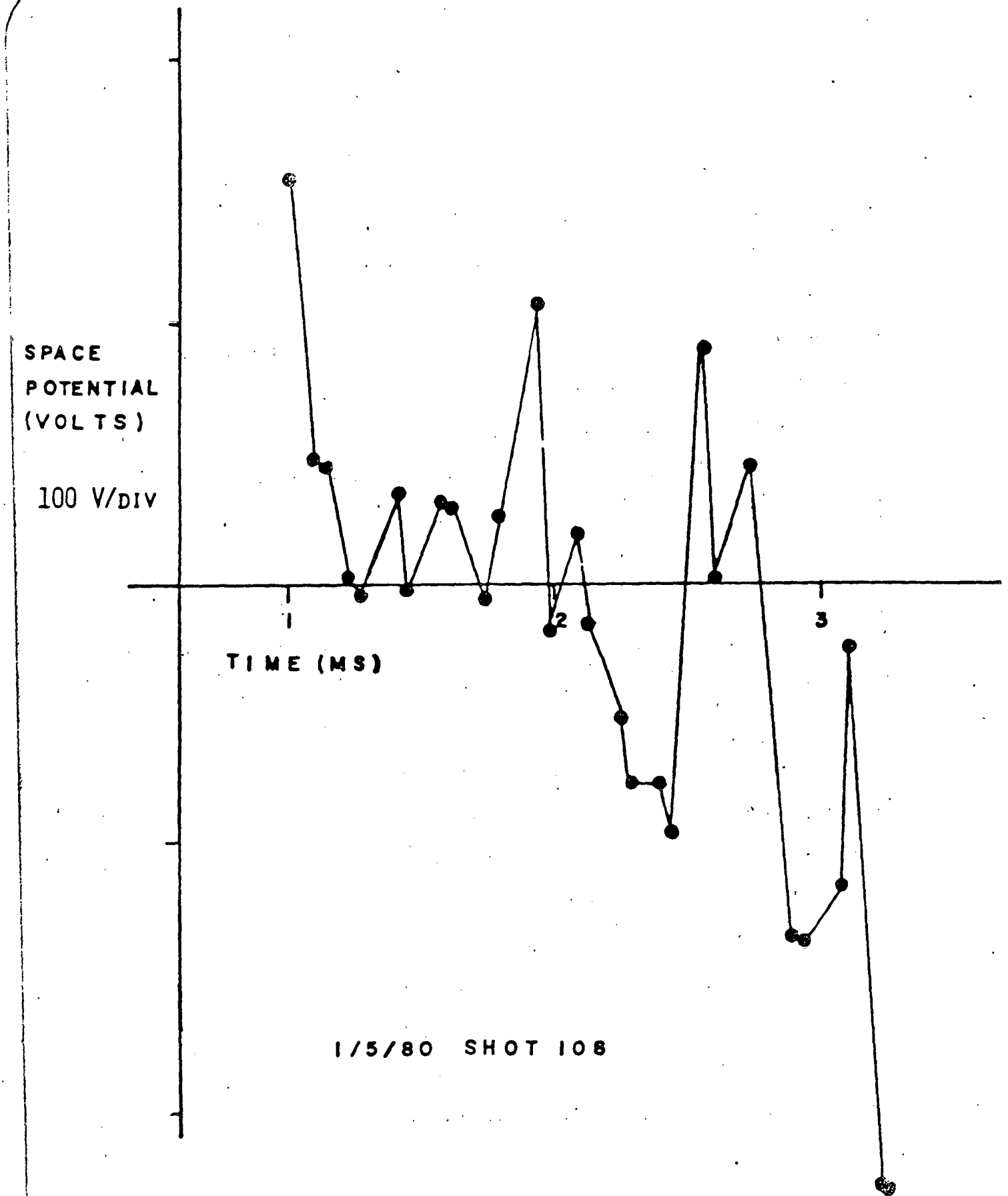

FIGURE 26

VI. SUMMARY

In summary we would like to note that beam probe systems can provide accurate, reliable measurements of plasma space potential and $nf(T_e)$. Over some temperature range, at least, it should be possible to separate n and T_e by measuring the multiple ionization reaction products. It is also an ideal diagnostic for studying fluctuations since it provides a simultaneous measurement of ϕ and $nf(T_e)$ from the same point in the plasma and the measurements are continuous in time. Measurements can be made quasi-continuously in space by rapidly sweeping the beam. By using more than one detector it should be possible to make measurements simultaneously at two different observation points in the plasma. And we hope to pursue space time correlation measurements in the near future.

It should also be noted that this report is only intended as a survey to illustrate the type of information that can be obtained with heavy ion beam probes. No attempt has been made to even point out some of the more detailed problems, such as spatial and temporal gradients over the sample volume or spatial and velocity variations in the probing beam. Beam probing is a sophisticated diagnostic that can provide large quantities of information about the plasma, but like all complex systems it requires a good deal of attention and a thorough understanding of its operation in order to correctly interpret the data. A continuous part of beam probing is very frequent testing and recalibration of the instrumentation and continuing simulation studies and trajectory calculations.

We believe that we have just started to scratch the possibilities of what can be done with beam probe diagnostic systems. This is summarized in

Fig. 27 where we have tried to indicate the various plasma parameters that it may be possible to investigate with particle beam probes and then indicate whether these parameters have actually been investigated in various types of magnetic geometries. As you can see there are lots of yes's for possibilities and lots of no's for actual implementation. So in summary a lot more work remains to be done.

TABLE 1

CAPABILITIES AND STATUS OF PARTICLE BEAM PROBES

Plasma Parameters	Are Particle Beams Sensitive?	Present Status of Diagnostic Technique				Are Other Techniques Available?
		TOKAMAK	EBT	MIRROR	OTHER	
$\phi(r)$	Yes	Yes[1]	Yes	Yes[2,3]	Yes	No
$N_e(r)$	Yes	Yes[1]	Yes[1]	Yes[2,3]	Yes[1]	Yes[4]
$T_i(r)$	?[8]	No	No	No	No	Yes[5]
$T_e(r)$	Yes	No	No[3]	No	Yes	Yes[3]
$J(r)$	Yes	Yes[6]	--	--	No	Yes[7]
$B(r)$	Yes	No	No	No	No	No
$\tilde{\phi}$	Yes	No[3]	No[3]	No[3]	Yes	No
$\tilde{N}_e$	Yes	Yes[1]	No	No	Yes	Yes[4]
$\tilde{T}_i$	?	No	No	No	No	No
Z_{eff}	Yes[6]	Yes[6]	No	No	No	Yes[4]
Fluctuation Correlations	Yes	No	No	No	Yes	No

[1] Refinement of technique in progress

[2] Demonstrated on central cell of TMX, but not in minimum B geometry

[3] Development of technique in progress

[4] No continuous spatially resolved technique

[5] Primarily charge exchange neutral, but requires a particle beam to obtain space resolution

[6] Light emission from Li neutral beam--PULSATOR; to obtain Z_{eff} have to assume Spitzer conductivity

[7] Modulated Thomson Scattering--DITE

[8] Need to know heavy ion-proton charge exchange cross-section

FIGURE 27

DISTRIBUTION LIST

Internal

K. A. Connor
R. L. Hickok
W. C. Jennings
J. F. Lewis
R. C. Rafun
J. T. Woo
R.P.D.L. Library
R.P.D.L. Graduate Students

External

P. Stone -- DOE
R. Taylor -- UCLA
J. C. Sprott -- U. of Wisconsin
J. L. Shohet -- U. of Wisconsin
M. Kristiansen -- Texas Tech
K. Gentile -- U. of Texas
E. Powers -- U. of Texas
J. L. Cecchi -- PPPL
F. C. Jobes -- PPPL
J. C. Glowienka -- ORNL
J. F. Pipkins -- General Atomic
K. McCormick -- Garching
J. Fujita -- Nagoya University
P. Vandenplas -- Ecole Royale Militaire
F. Cap -- U. of Innsbruck
R. K. Feeney -- Georgia Tech
A. Dellis -- Culham Lab
W. Ard -- McDonnell Douglas
P. Colestock -- PPPL
H. Fleishman -- Cornell
K. Moses -- TRW
J. R. Roth -- U. of Tennessee
P. Willis -- GE
D. Priester -- DOE
C. Damm -- LLL
P. Demchenko -- Kharkov
L. Krupnik -- Kharkov
V. Tershin -- Kharkov
V. Yakubouski -- Kharkov